

URBAN ANALYTICS ON GREEN COVERAGE IN MALAYSIA WITH STREET  
VIEW IMAGES

CHONG XIAN JUN

UNIVERSITI TEKNOLOGI MALAYSIA



## UNIVERSITI TEKNOLOGI MALAYSIA

**DECLARATION OF THESIS / UNDERGRADUATE PROJECT REPORT AND  
COPYRIGHT**

Author's full name : CHONG XIAN JUN

Date of Birth : 14/07/1998

Title : URBAN ANALYTICS ON GREEN COVERAGE IN MALAYSIA  
WITH STREET VIEW IMAGES

Academic Session : 2022/2023

I declare that this thesis is classified as:

☐**CONFIDENTIAL**(Contains confidential information under the  
Official Secret Act 1972)\*☐**RESTRICTED**(Contains restricted information as specified by the  
organization where research was done)\*☒**OPEN ACCESS**I agree that my thesis to be published as online  
open access (full text)

1. I acknowledged that Universiti Teknologi Malaysia reserves the right as follows:
2. The thesis is the property of Universiti Teknologi Malaysia
3. The Library of Universiti Teknologi Malaysia has the right to make copies for the purpose of research only.
4. The Library has the right to make copies of the thesis for academic exchange.

Certified by:

---

**SIGNATURE OF STUDENT**

---

MCS211047

---

---

**SIGNATURE OF SUPERVISOR**

---

TS. DR. CHAN WENG HOWE

---

Date: 12 JANUARY 2023

Date: 12 JANUARY 2023

NOTES : If the thesis is CONFIDENTIAL or RESTRICTED, please attach with the letter from the organization with period and reasons for confidentiality or restriction



“I hereby declare that I have read this proposal and in my opinion this proposal is sufficient in term of scope and quality for the award of the degree of Master of Science (Data Science).”

Signature : \_\_\_\_\_  
Name of Supervisor I : TS. DR. CHAN WENG HOWE  
Date : 12 JANUARY 2023



## **BAHAGIAN A - Pengesahan Kerjasama\***

Adalah disahkan bahawa projek penyelidikan tesis ini telah dilaksanakan melalui kerjasama antara \_\_\_\_\_ dengan \_\_\_\_\_

Disahkan oleh:

Tandatangan :

Tarikh :

Nama :

Jawatan :

(Cop rasmi)

*\* Jika penyediaan tesis atau projek melibatkan kerjasama.*

---

## **BAHAGIAN B - Untuk Kegunaan Pejabat Sekolah Pengajian Siswazah**

Tesis ini telah diperiksa dan diakui oleh:

Nama dan Alamat Pemeriksa Luar :

Nama dan Alamat Pemeriksa Dalam :

Nama Penyelia Lain (jika ada) :

Disahkan oleh Timbalan Pendaftar di SPS:

Tandatangan :

Tarikh:

Nama :





URBAN ANALYTICS ON GREEN COVERAGE IN MALAYSIA WITH STREET  
VIEW IMAGES

CHONG XIAN JUN

A proposal submitted in partial fulfilment of the  
requirements for the award of the degree of  
Master of Science (Data Science)

Faculty of Computing  
Universiti Teknologi Malaysia

JANUARY 2023



## DECLARATION

I declare that this proposal entitled “URBAN ANALYTICS ON GREEN COVERAGE IN MALAYSIA WITH STREET VIEW IMAGES ” is the result of my own research except as cited in the references. The proposal has not been accepted for any degree and is not concurrently submitted in candidature of any other degree.

Signature : .....  
Name : CHONG XIAN JUN  
Date : 12 JANUARY 2023

## **DEDICATION**

This thesis is dedicated to my father, who taught me that the best kind of knowledge to have is that which is learned for its own sake. It is also dedicated to my mother, who taught me that even the largest task can be accomplished if it is done one step at a time.

## **ACKNOWLEDGEMENT**

In preparing this project proposal, I am very much indebted to my supervisor Ts. Dr. Chan Weng Howe for his useful advice. I would also love to express my gratitude for my friends who had helped me out in this project.

## **ABSTRACT**

This research project addresses the lack of research on urban green coverage in Malaysia, especially from the perspective of human users. With green view index (GVI), a metric that quantifies the visibility of green spaces from specific locations, this project investigated the distribution of green views in a representative sample area of Johor Bahru city centre, Malaysia. The project utilizes pixel segmentation methods and deep learning models (specifically, the DCNN end-to-end model and DeepLabV3+ model) to predict the GVI in study site using street view images from Google Street View (GSV). The findings reveal that the DCNN end-to-end model demonstrates the highest accuracy for GVI prediction, exhibiting the lowest mean absolute error of 4.58% and the highest Pearson correlation coefficient of 0.97 compared to the pixel segmentation and DeepLabV3+ models (6.78%, 0.94 and 6.71%, 0.92, respectively). Moreover, the DCNN end-to-end model shows to have higher robustness for its predictions with the smallest range of GVI estimation error (5-95%) at 0.16 (-0.067116, 0.087973) compared to the other models. The study generates insights into the distribution and quality of urban green spaces by mapping the predicted GVI values onto a dashboard, enabling the comprehension of urban green coverage and the identification of spatial patterns. This research outcome, communicated through a Microsoft PowerBI dashboard, contributes to the application of deep learning as a valuable tool for understanding urban green spaces in Malaysia and supports urban planning and decision-making processes in the context of sustainable development.

## ABSTRAK

Projek penyelidikan ini menangani kekurangan penyelidikan mengenai ruang hijau bandar di Malaysia, terutamanya dari perspektif pengguna manusia. Dengan menggunakan indeks pandangan hijau (Green View Index atau GVI), satu metrik yang mengukur kebolehlihatan ruang hijau dari lokasi tertentu, projek ini mengkaji taburan pandangan hijau di kawasan sampel yang mewakili pusat bandar Johor Bahru, Malaysia. Projek ini menggunakan kaedah pengasingan piksel dan model pembelajaran mendalam (khususnya, model DCNN end-to-end dan model DeepLabV3+) untuk meramalkan GVI di lokasi kajian menggunakan imej pandangan jalan dari Google Street View (GSV). Hasil kajian menunjukkan bahawa model DCNN end-to-end menunjukkan ketepatan tertinggi dalam meramalkan GVI, dengan kesalahan min mutlak terendah pada 4.58% dan pekali korelasi Pearson tertinggi pada 0.97 berbanding model pengasingan piksel dan model DeepLabV3+ (6.78%, 0.94 dan 6.71%, 0.92, masing-masing). Selain itu, model DCNN end-to-end juga menunjukkan ketahanan yang lebih tinggi dalam meramalkan GVI dengan julat terkecil bagi kesalahan anggaran GVI (5-95%) pada 0.16 (-0.067116, 0.087973) berbanding dengan model-model lain. Kajian ini menghasilkan wawasan mengenai taburan dan kualiti ruang hijau bandar dengan memetakan nilai-nilai GVI yang diramalkan pada suatu papan pemuka, membolehkan pemahaman tentang liputan ruang hijau bandar dan pengenalan corak spatial. Hasil penyelidikan ini, yang disampaikan melalui papan pemuka Microsoft PowerBI, memberi sumbangan kepada penggunaan pembelajaran mendalam sebagai alat penting untuk memahami ruang hijau bandar di Malaysia dan menyokong proses perancangan bandar dan pembuatan keputusan dalam konteks pembangunan mampan.

## TABLE OF CONTENTS

	TITLE	PAGE
	<b>DECLARATION</b>	<b>iii</b>
	<b>DEDICATION</b>	<b>iv</b>
	<b>ACKNOWLEDGEMENT</b>	<b>v</b>
	<b>ABSTRACT</b>	<b>vi</b>
	<b>ABSTRAK</b>	<b>viii</b>
	<b>TABLE OF CONTENTS</b>	<b>viii</b>
	<b>LIST OF TABLES</b>	<b>xi</b>
	<b>LIST OF FIGURES</b>	<b>xii</b>
	<b>LIST OF EQUATIONS</b>	<b>xii</b>
	<b>LIST OF ABBREVIATIONS</b>	<b>xvi</b>
<b>CHAPTER 1</b>	<b>INTRODUCTION</b>	<b>1</b>
1.1	Problem Background	1
1.2	Problem Statenment	2
1.3	Research Questions	3
1.4	Aim and Objectives	3
1.5	Scope of Study	4
1.6	Significance of Study	5
1.7	Project Organization	5
<b>CHAPTER 2</b>	<b>LITERATURE REVIEW</b>	<b>7</b>
2.1	Overview of Literature Review	7
2.2	Research on Urban Greeneries in Malaysia	8
2.3	Green View Index (GVI) with Street Views	9
2.4	GSV Configurations for Street View Collection	12
2.5	Prediction Model for Green View Index (GVI)	14
2.5.1	Pixel Segmentation Model	14



2.5.2	Deep Learning Models to Predict GVI	15
2.5.2.1	DCNN End-to-End Model	19
2.5.2.2	HRNet-OCR Model	20
2.5.2.3	DeepLabV3+ Model	23
2.6	Performance Measure for GVI Prediction	24
2.7	Interpretation of GVI	26
2.6	Issues	27
<b>CHAPTER 3</b>	<b>RESEARCH METHODOLOGY</b>	<b>29</b>
3.1	Research Framework	29
3.2	Data Preparation	31
3.2.1	Data Collection	31
3.2.1.1	Sampling Street View Data	31
3.2.1.1	Cityscape Data Collection	35
3.2.2	Data Preprocessing	36
3.2.2.1	Data Preprocessing GSV	36
3.2.2.2	Data Preprocessing for Cityscape Data	37
3.2.3	Splitting Data for Model Development	38
3.3	Model Development for GVI Prediction	39
3.3.1	Pixel Segmentation Model	39
3.3.2	Deep Learning Models	42
3.4	Evaluation of Models	44
3.4.1	Pixel Segmentation Model	45
3.4.2	Deep Learning Models	45
<b>CHAPTER 4</b>	<b>RESULTS AND DISCUSSION</b>	<b>47</b>
4.1	Model Performance for GVI Computation	47
4.1.1	Accuracy Evaluation	48
4.1.2	Robustness Evaluation	48
4.1.3	Inference Time Evaluation	50
4.1.4	Bias Analysis for Prediction Models	50
4.2	Visualization of GVI Prediction in Study Site	51
4.3	Clustering Analysis of GVI	53

4.3.1	Cluster 0	56
4.3.2	Cluster 1	58
4.3.3	Cluster 2	60
4.3.4	Cluster 3	63
4.3.5	Clustering Analysis Conclusion	65
4.4	Dashboard	67
4.4	Chapter Summary	<u>70</u>
<b>CHAPTER 5</b>	<b>CONCLUSION AND RECOMMENDATIONS</b>	<b>71</b>
5.2	Contributions	71
5.1	Limitations	72
5.2	Future Improvements	73
<b>REFERENCES</b>		<b>745</b>

## LIST OF TABLES

<b>TABLE NO.</b>	<b>TITLE</b>	<b>PAGE</b>
Table 2.1	Examples of other GVI studies and their applications.	10
Table 2.2	Different configurations of GSV.	12
Table 2.3	Summary of the deep learning models used to compute GVI.	16
Table 2.4	Accuracy comparison between different models.	17
Table 3.1	The metadata of sampled images.	28
Table 4.1	Accuracy comparison between different models for GVI computation.	35
Table 4.2	DCNN KMeans clusters with their respective mean GVI predictions.	39

## LIST OF FIGURES

<b>FIGURE NO.</b>	<b>TITLE</b>	<b>PAGE</b>
Figure 1.1	Site plan boundary.	4
Figure 2.1	Example of green pixels that are not actual greenerie	14
Figure 2.2	Diagram illustrating working principles of CNN.	15
Figure 2.3	Building block of residual network.	15
Figure 2.4	Residual network architecture diagram vs plain network.	15
Figure 2.5	HRNet basic architecture diagram.	15
Figure 2.6	OCR basic architecture diagram.	15
Figure 2.7	Components and basic architecture to develop DeepLabV3+ model.	23
Figure 2.8	Illustration of the intersection over union (IOU)	24
Figure 2.9	Map plots of GVI for Amsterdam and Singapore as an illustration.	26
Figure 3.1	Project research framework.	24
Figure 3.2	Study site plan with boundaries.	26
Figure 3.3	Sample view collected from a sample point at (1.4574946, 103.7690224).	27
Figure 3.4	Map plot of sampled locations.	26
Figure 3.5	The street view image and its complementary segmentation label image from Cityscape dataset.	26
Figure 3.6	A sample of the street view image and its target mask.	30
Figure 3.7	The process of Pixel Segmentation for green vegetation extraction and GVI calculation.	32
Figure 3.8	The process to develop deep learning models to predict GVI.	33
Figure 4.1	GVI prediction error for the 3 models studied.	37
Figure 4.2	The frequency of underestimation and overestimation of model and bias investigation for 3 models.	38
Figure 4.2	The frequency of underestimation and overestimation of model and bias investigation for 3 models.	38

Figure 4.3	Dashboard visualising the GVI predictions on target site.	38
Figure 4.4	Distributions of GVI predictions with 3 different models.	38
Figure 4.5	Kmeans clustering for GVI predictions based on DCNN, DeepLabV3+ and Pixel Segmentation model.	38
Figure 4.6	Agglomerative clustering for GVI predictions based on DCNN, DeepLabV3+ and Pixel Segmentation model.	38
Figure 4.7	Scatterplot latitude, longitude, mean GVI predictions on 3D-space to see if the data distribution is spherical.	38
Figure 4.8	Determine the number of clusters with elbow method.	38
Figure 4.9	Visualization of hierarchical clusters (DCNN, cluster=4).	38
Figure 4.10	Visualization of cluster 0 for DCNN Kmeans clustering	38
Figure 4.11	Roads that intersect with or adjacent to spots from cluster 0.	38
Figure 4.12	Sample GSV images taken from highways and main roads with very little observable vegetation.	38
Figure 4.13	Highlights on the city center with high density commercial area.	38
Figure 4.14	Sample GSV images taken from areas highlighted in Figure 4.13.	38
Figure 4.15	Visualization of cluster 1 for DCNN Kmeans clustering.	38
Figure 4.16	Indication of the sampling location for GSV images displayed in Figure 4.17 and Figure 4.18.	38
Figure 4.17	Sample GSV images from commercial areas marked in Figure 4.16.	38
Figure 4.18	Sample GSV images from residential areas marked in Figure 4.16.	38
Figure 4.19	Visualization of Cluster 2 for DCNN Kmeans clustering.	38
Figure 4.20	displays the aerial view and grayscale map where Cluster 3 points are plotted on.	38
Figure 4.21	Indication of the sampling location for GSV images displayed in Figure 4.22.	38
Figure 4.22	Sample GSV images marked in Figure 4.20.	38
Figure 4.23	GSV image of the street incorporating street trees in the walkway on the Chinatown street. Its location is marked on the map on the left.	38

Figure 4.24	Visualization of Cluster 3 for DCNN Kmeans clustering.	38
Figure 4.25	Comparison of Cluster 3 (right) distribution compared with Cluster 2 (left).	38
Figure 4.26	Indication of the sampling location for GSV images displayed in Figure 4.27.	38
Figure 4.27	Sample GSV images marked in Figure 4.26.	38
Figure 4.28	This dashboard investigates the error of each model at different predicted GVI values.	38
Figure 4.29	This dashboard visualizes the GSV image and label to allow more detailed error analysis of model with visual inspection.	38
Figure 4.30	This dashboard visualizes the GVI predictions of all GSV data collected on site.	38

## LIST OF EQUATIONS

FIGURE NO.	TITLE	PAGE
Equation (2.1)	The formula to calculate GVI.	10
Equation (2.2)	The formula to calculate IOU.	19
Equation (2.3)	The formula to calculate RMSE.	19
Equation (2.4)	The formula to calculate MAE.	19
Equation (2.5)	The formula to calculate Pearson correlation coefficient ( r ).	20
Equation (2.6)	The formula to calculate sGVI.	21
Equation (3.1)	The formula to limit random sample points within 1000m radius from the center coordinates of site (JBCC Komtar).	26
Equation (3.2)	The formula to calculate GVI.	30

## LIST OF ABBREVIATIONS

API	-	Application Programming Interface
CNN	-	Convolutional Neural Network
FCN	-	Full Convolutional Network
GSV	-	Google Street View
GVI	-	Green View Index
HRNet- OCR	-	High-Resolution Net- Object Contextual Representations
IOU	-	Intersection over Union
MAE	-	Mean Absolute Error
ResNet	-	Residual Neural Network
RMSE	-	Root Mean Squared Error
sGVI	-	Standardised Green View Index
TSV	-	Tencent Street View



# CHAPTER 1

## INTRODUCTION

### 1.1 Problem Background

Urban greens, including trees, shrubs, and associated vegetation in cities, have long been recognized for their importance in the urban environment. In fact, there have been countless studies in recent years reiterating the instrumental importance of urban forests or trees in lowering urban temperatures and creating more comfortable microclimates (Pauliet, 2003; Schwaab, 2021), providing physical and mental health benefits (Lee, 2010), etc. making the urban areas more livable for its inhabitants.

Unfortunately, there are hardly any regulations guiding the management of urban greens in Malaysia. The Malaysian urban landscape planning practices are mostly based only on open space coverage (Rusli and Rudin, 2010). For instance, under the National Urbanization Policy (NUP), two hectares of open space per 1000 urban population were set as the planning standard and a minimum of 10% or 0.2 hectares of open spaces are dedicated for all development (NUP9.ii). While open spaces are an essential part of urban greens, this single variable on itself is not enough to provide comprehensive data to inform planning that can optimize the experience of the places' inhabitants.

Along with the increase in global awareness on the importance in urban green spaces, urban green space is increasingly seen as an integral part of cities planning (James, 2009), fueling the growth of research in this field. According to the systemic review based on PRISMA framework by Rajoo et. al. (2021), there is a growing trend in research articles concerning urban forests in Malaysia from 2007 onwards. Out of the 43 records reviewed, only 4 of them were focused on the spatial analysis of urban green space (Kanniah, 2017; Masum et. Al., 2017; Kasim et. Al., 2019, Nor

et. Al., 2019). This shows an untapped opportunity where the spatial analysis on urban green coverage in Malaysia can be investigated.

Nevertheless, all of the spatial studies are based on macro-scale aerial views, making them not representative of the human experience on the ground level on the day-to-day micro level. While these studies are essential, they are not able to relate to the direct human user perspectives when they are in the city. In other words, satellite imagery is useful for high level planning of preservation and restoration, but not informative for the environmental design of the everyday human experience.

It is long overdue that we adopt better metrics to measure urban greeneries coverage that can allow us to integrate urban green into our daily experience in the Malaysian urban environment.

## **1.2 Problem Statement**

In this study, we try to tackle the problem by measuring and mapping urban green in a Malaysian city to analyze its coverage from the eyes of the users. In other words, this study measures: “how much greeneries can people in a Malaysian city see?”

The quantified study of the urban users’ views is made possible by the establishment of Green View Index (GVI), which makes use of street view images and detects the proportion of greeneries in the images collected. While the study is limited to the street views, the studies and information extracted remain to be highly informative for planners as the streets are the public space with the most human activity.

Nevertheless, there are several challenges to overcome in the study, which lead to our research questions.

### **1.3 Research Questions**

The questions that this research attempts to answer are:

1. How do we collect the large amount of street view data required as raw data and study the urban green coverage?
2. Given the large amount of street view images, what kind of learning algorithms can we use to predict GVI efficiently?
3. How do we interpret and analyze the predicted GVI and make it informative for the urban planning process?

### **1.4 Aim and Objectives**

The aim of this project is to visualize the state of urban green coverage in Malaysian city from the users' perspective with Green View Index (GVI). Dashboard is developed as the final output that allows us to interpret the findings intuitively. Objectives of this research are as follow:

1. To collect and process street view images data to measure urban green coverage from the perspective of human users.
2. To compute GVI effectively from street view images with Pixel Segmentation and supervised machine learning models.

3. To develop a dashboard to visualize the estimated GVI of selected sites and assess the distribution of green views in Malaysian city.

## 1.5 Scope of Study

Due to limitations in time and resources, a smaller scope in Johor Bahru city center is chosen as a representative sample site for this study. It is chosen due to it being the central hub of Johor Bahru with a high population density. As there are no official boundaries demarcating the Johor Bahru city center area, local experience is used to help formulate the definition of city center area. In this case, the main road *Jalan Lingkaran Dalam* acts as the edge of the city center.

Meanwhile, the street views images used to compute GVI are collected in December 2022 from the Street View API provided by Google Maps due to its availability and accessibility. As the site has a nearly eclipse outline, the actual boundary of the studied site is approximated by a circle to facilitate the function of Google Maps. With several experimentations, the sample site is set to be a circle with a 1000m radius from the *Komtar JBCC*.

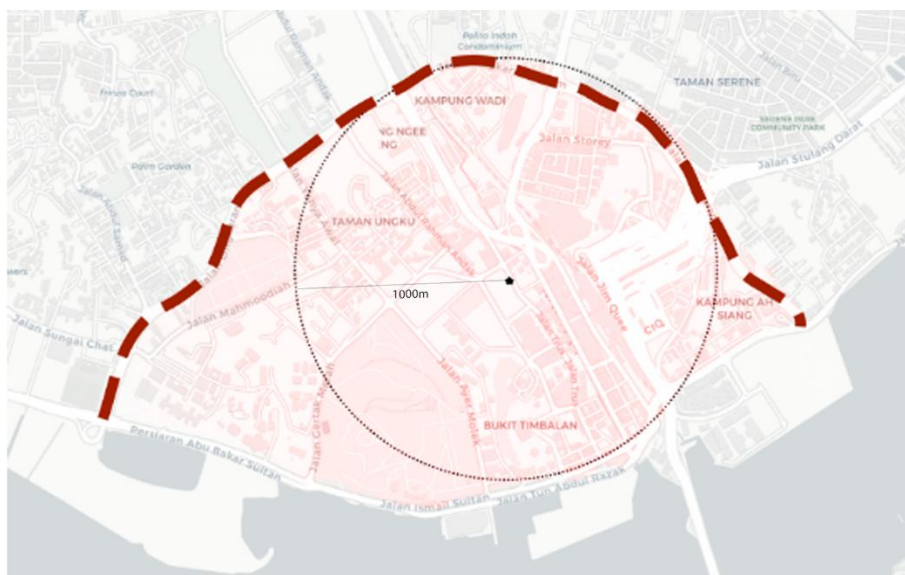


Figure 1.1 Site plan boundary.

## **1.6 Significance of Study**

The project is expected to provide comprehensive insights on the urban green coverage from users' perspectives measured by GVI in Johor Bahru city centre. This information will be useful to discover the state of urban green coverage in a Malaysian city and inform the process of urban planning of the said area, while also shining some light on the conditions of the other similar urban areas in Malaysia.

Besides, this study also seeks to compare various existing methods used to compute Green View Index (GVI) to find out the most accurate methods for the task.

## **1.7 Project Organization**

The project is laid out in 5 chapters, in the first chapter we go through the introduction to the problem background and statement, research questions and objectives, along with the scope to establish the framework of study. In Chapter 2, extensive literature review is done to understand the state of urban greeneries research in Malaysia, the use of GVI and the methods used to compute GVI. Several methods are reviewed, and their respective evaluation metrics are explored. In Chapter 3, detailed methodology for the project procedure is established, from data preparation to model development and evaluation, and lastly reporting. Chapter 4 cover initial findings about GVI in the study site. Chapter 5 concludes the project with its achievements, limitations and how it can be improved.



## **CHAPTER 2**

### **LITERATURE REVIEW**

#### **2.1 Overview of Literature Review**

By and large, urban greeneries in Malaysia are managed only very indirectly through the management of open space coverage. However, this is hardly an effective measure to optimize the effects of tree coverage in the urban environment. Thus, various studies on urban forests were published to investigate various effects of urban greeneries, e.g. in ecology, biodiversity, accessibility, etc. In this project, the Green View Index (GVI) measured by using street view images along with machine learning algorithms is proposed as another metric to augment the urban planning process in Malaysia.

While previous studies have successfully established the methods to measure and compute GVI in cities, there is still room for improvements in this area, particularly in the context of Malaysian urban areas.

In this literature review, we will study the research questions in several different sections. Firstly, we will establish the background context by reviewing the existing studies of urban greeneries coverage in Malaysia. Later, we dive into the literature discussing the importance and the methods to measure GVI. Lastly, algorithms and models developed in previous studies to detect and compute GVI from the street views are explored to find out the most efficient way to adopt for this project. The extracted insights will provide a foundation for our study, which aims to investigate the GVI measurement in Johor Bahru city center.

## **2.2 Research on Urban Greeneries in Malaysia**

In Malaysia, the management of urban greeneries are based crudely on the measurement of open and green space (land specified as public area, loosely correlated with green area) coverage according to the Department of Town and Country Planning, Peninsular Malaysia (JPBD). Several standards are established, e.g., 2 hectares of open space are reserved for each 1000 urban populations, green areas to be established as buffer zones to limit urban development. While these measurements are essential for sustainable urban planning, they are not sufficient to optimize the urban greeneries.

While there is a lack of urban greeneries management practice, there are various research being done in Malaysia attempting to fill in the gap. In a systematic review done on urban forestry research with PRISMA framework (Rajoo et. al., 2021), there is a consistent growth in the research concerning urban forests in Malaysia from 2007 onwards. Nevertheless, out of the 43 records reviewed, only 4 of them were focused on the spatial analysis of urban green space (Kanniah, 2017; Masum et. Al., 2017; Kasim et. Al., 2019, Nor et. Al., 2019). This shows an untapped opportunity where the spatial analysis on urban green coverage in Malaysia can be investigated.

On the topic of urban green spatial analysis in Malaysia, the research done are typically conducted based on aerial images on macro or micro planning scale. For instance, on a high-level master planning scale, Kasim et. al. (2019) published a study that documented the changes in urban green spaces between 2002, 2012 and 2017 with the use of high-resolution aerial imagery; Kanniah (2017) made use of time-series Landsat satellite imagery to monitor green cover changes in Kuala Lumpur from 2001 to 2016. On the lower-level planning, Ludin and Rusli (2009) monitored the quality and distribution of open spaces in Johor Bahru Tengah Municipal Council with remote sensing data.

However, all of the studies mentioned above are investigated with aerial top-down view for instrumental planning. However, top-down view studies are abstract



and not directly informative for the environmental design of the everyday human experience, making it not relatable to the end-user experience. To the best of our knowledge, there is no objective study done from the perspective of urban environment users, which is a crucial measurement central to the planning of experience of the users in the urban environments. This leaves a research opportunity for such a project to happen.

### **2.3 Green View Index (GVI) with Street Views**

Conventionally, aerial remote data has been used for the task of trees mapping or any other similar land surveying tasks. Even with the advancement of new techniques such as remote sensing methods such as LiDAR, aerial top-down view remains to be the main perspective in which urban greeneries coverage is measured. However, we have all known that the top-down view is hardly how we humans experience our environment as we perceive it in a perspective view, making the studies being hard to relate for the end-user experience of urban dwellers. This is especially relevant in urban environments where man-made facilities are juxtaposed with the mixture of trees, forming urban treescapes with massively different appearances for the same green area.

Many studies have attempted to study the visual impact of urban trees. However, a lot of them were qualitative and subjective in nature (J. Yang et. al., 2009). One of the most popular methods used were ranking, in which the participants of the survey were shown pictures or videos of urban forests and requested to score the pictures. It does not take much to understand the limitations of the studies: qualitative, subjective and unscalable. J. Yang et. al. (2009) established a new metric called Green View Index (GVI) which measures the amount of greenery that people can see on the ground at different locations in a city, laying the foundation for all the future quantified studies of visual effect of urban treescapes.

The index calculation was simple but ingenious. On strategically sampled points on a target site, eye-level photographs were taken at each point and the GVI

index of each point was then interpreted by calculating the ratio between areas containing foliage over the areas of whole photos. In short, it can be defined as the ratio of greenery within the people's field of view with a range between 0 and 1, of which 0 represents no greeneries at all and 1 means that the image is full of greeneries. Due to the streets being the main public space where urban dwellers experience, Green View Index (GVI) is typically measured by using images taken from the street. The formula to calculate GVI is shown in Equation (2.1) below. M refers to the total number of horizontal directions taken on a single point, N refers to the number of vertical view angles for each sample site;  $Area_g$  refers to the area of a GSV image covered by greeneries, while  $Area_t$  refers to the total area of a single GSV image.

$$GVI = \frac{\sum_{j=1}^N \sum_{i=1}^M Area_g}{\sum_{j=1}^N \sum_{i=1}^M Area_t} \quad (2.1)$$

Equation (2.1) shows the formula to calculate GVI.

After the establishment of GVI, it has since become the foundation for future researchers to conduct quantitative studies on urban treescapes for landscape and urban planning studies. With the development of services like Google Street View, GVI has become even more viable as a technique to map urban green view and become an increasingly popular metric for urban green space research. Table 2.1 displays several examples of the use of GVI in various studies and their applications.

Table 2.1 Examples of other GVI studies and their applications.

Application	Study	Discussion
Investigate green view distribution	View-based greenery: A three-dimensional assessment of city buildings' green visibility using Floor Green View Index (Yu et. al. 2016)	GVI is modified to Floor Green View Index (FGVI) to quantify the area of visible urban vegetation from a certain floor of building.
	How green are the streets? An analysis for central areas of Chinese cities using Tencent Street View (Long and Liu, 2017)	Analyze street greeneries in 245 central area in Chinese Cities and detect patterns of street green view distribution.
	Treepedia 2.0: Applying Deep Learning for Large-scale Quantification of Urban Tree Cover (Cai et. al., 2018)	Develop deep learning method to compute GVI with significantly higher accuracy.
City walkability	Analyzing the effects of Green View Index of neighborhood streets on walking time using Google Street View and deep learning (Ki and Lee, 2021)	Use deep learning to compute GVI and find out its relationship with walking time.
Socioeconomic investigation	Who lives in greener neighborhoods? The distribution of street greenery and its association with residents' socioeconomic conditions in Hartford, Connecticut, USA (Li et. al., 2015)	Aggregate GVI at the block group level to compare differences in GVI based on the socioeconomic status of an area.

## **2.4 GSV configurations for Street Views Collection**

One of the greatest limitations of J. Yang et. al.'s study was the excessive resources required for data collection on large scale as it involved extensive manual labor to take street view photos. With the advancement of mapping services, it has become a lot easier for us to retrieve our needed street view images via Google Street View API without needing to manually take the photos of tree coverage on the street. Other than the ability to collect a larger amount of data easily, the use of Google Street View (GSV) also allows us to be more precise on our camera settings to get unbiased data for urban street treescape mapping. However, the use of GSV requires its users to have a clear understanding on the image taking configurations for the image collection.

One of the good references for this is the street-level urban greenery assessment conducted by Li et. al., 2017. They sampled 258 points of street view data collection randomly across its study site, with at least 100m intervals on average between each point. To ensure each sampling point includes all the green areas that a pedestrian can possibly see, they took 3 panoramic views upwards, straight and downwards. In the Google Street View API parameters, the “heading” was set to 0, 60, 120, 180, 240, and 300 respectively to capture a full 360-degree panorama; the “pitch” was set to -45, 0, and 45 to capture different views and 18 images were taken at each sampling point.

In fact, other than the method mentioned above, there have been many street view image configurations used in different research for different purposes. Dong et. al. (2018) reviewed multiple street view configurations used by previous research. In their review, they used Tencent Static Image (TSV) service to simulate all the GSV configurations coming up in other research.

Table 2.2 Different configurations of GSV

Configuration Name	Description	Discussion
GVI4	GVI computed with 4 horizontal TSV images with heading angle of 90°. (Long and Liu, 2017)	Greater numbers of headings allow for a lower field of vision (zoomed in), but also takes up more computational resources to compute.
GVI	GVI computed with 6 horizontal TSV images with heading angle of 60°. (Zhang and Dong, 2018)	
GVI8	GVI computed with 8 horizontal TSV images with heading angle is 45° (Dong et. al., 2018)	
GVI18	Similar approach as method used by Li et. al. GVI computed with 6 horizontal TSV images with heading angle of 60° and 3 pitches for each heading. 18 images taken in total. (Li et. al., 2015)	Very comprehensive, but computationally expensive.
PGVI	GVI computed with cylindrical panorama stitched together from 6 horizontal TSV pictures. The distortion for PGVI might affect accuracy of GVI. (Cheng et. al., 2017)	Cylindrical panorama cause distortion in views.

While there are many configurations used, it is important that one experiments with different configurations and chooses a configuration that can minimizes distortion and overlap to reduce error in GVI estimation.

## **2.5 Prediction Models for GVI**

Yang et. al. (2009) made GVI calculations by manually selecting areas containing foliage using Adobe Photoshop selection, which is time and resource consuming and requires lots of automation.

### **2.5.1 Pixel Segmentation Model**

Li et. al. (2015) assessed the tree coverage in each image by extracting the green pixels with the Pixel Segmentation method, As pixels consisting of vegetation have typically higher reflectance values in the green band than red and blue, pixels consisting of greeneries can be extracted by selecting only the pixels with higher values in green band than red and blue. Nonetheless, it risks inaccuracies by including non-tree green objects and omitting shaded parts of trees that appears to be not green enough.



Figure 2.1 example of green pixels that are not actual greeneries.

### 2.5.2 Deep Learning Models to Predict GVI

With the advancement of deep learning and computer vision models, semantic segmentation can be deployed to detect and mask the greeneries in street view images effectively. One of the most common deep learning algorithms for the task is convolutional neural network (CNN). Convolutional neural networks (CNNs) are a type of specialized neural network for processing data with a grid-like topology (LeCun et al., 1997) that have been widely used for image classification and other computer vision tasks by learning hierarchical representations of the data through the use of convolutional layers (Katole et al., 2015).

The basic building block of CNN is a convolutional layer. It extracts features from the input data by applying a set of learnable filters to the input data. These filters are designed to learn different features at different scales, such as edges, corners, textures, and patterns to produce a set of feature maps. By stacking up the convolutional layers in a neural network, the architecture allowed the use of hierarchical representations to effectively capture the spatial relationships between

pixels in an image and learn complex patterns and features by itself as shown in Figure 2.2.

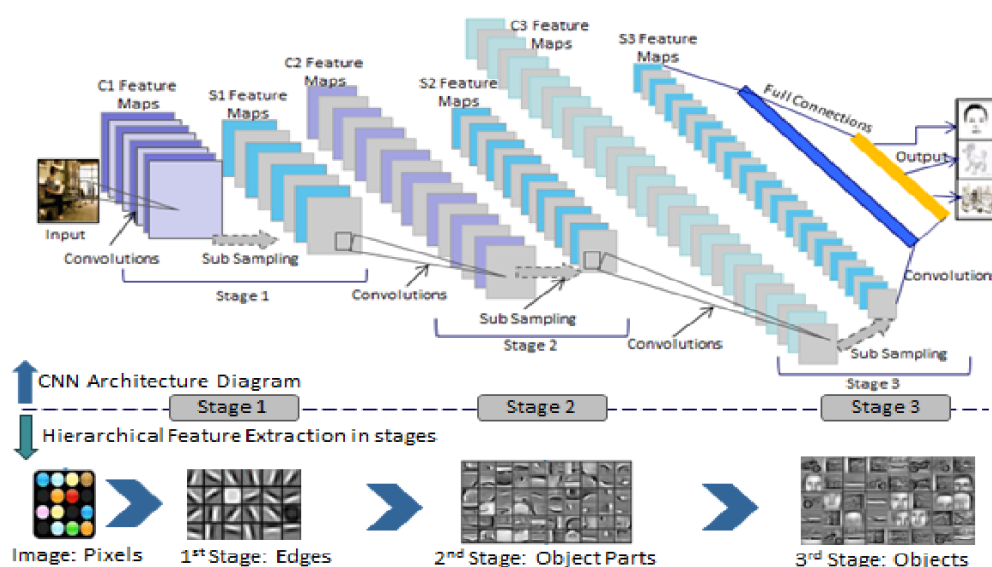


Figure 2.2 Diagram illustrating working principles of CNN.

Source: <https://www.semanticscholar.org/paper/Hierarchical-Deep-Learning-Architecture-For-10K-Katole-Yellapragada/f78e280123b1c0c68f84da3cc6c66615f6e7cebd/figure/0>

On top of CNN, many deep learning models are developed for image segmentation, e.g. ResNet (He et. al., 2017), FCN (Long et. al., 2015), SegNet (Badrinarayanan et. al., 2017), etc.

While CNN is the most commonly used architecture for image segmentation, there are many different models based on different architecture as well. For instance, recurrent neural networks (RNNs) based models, attention-based models, encoder-decoder based models, and others (Minaee et. al., 2022). As there are too many deep learning models developed for image segmentation, it is beyond the scope of this study to conduct an exhaustive review on every single model. So, this review will include only models that have been used to compute GVI.



Table 2.3 Summary of the deep learning models used to compute GVI.

Model	Method	Training and Calibration	Prediction Output
DCNN semantic segmentation (Cai et. al., 2018)	Pyramid Scene Parsing Network (PSPNet) (Zhao et. al., 2016) with 65,818,363 parameters	Pre-trained on full Cityscapes dataset, then trained on Cityscapes dataset, and finally on 320 GSV images collected by Cai et. al.	Pixel-segmented GSV image
DCNN end-to-end (Cai et. al., 2018)	Deep Residual Network (ResNet) (He et. al., 2017) with 28,138,601 parameters	Pre-trained on ImageNet dataset, then trained on Cityscapes dataset, and finally on 320 GSV images collected by Cai et. al.	Single GVI value between 0 and 1
HRNet-OCR (Zhang and Hu, 2022)	HRNet-OCR model (Yuan et. al., 2019) with 10,500,000 parameters	Trained on Cityscape dataset without calibration	Pixel-segmented GSV image
FCN-8 (Yu et. al., 2021)	Details of models not provided	Trained on ADE20K dataset, fine tuned with GSV images collected by author.	Pixel-segmented GSV image
DeepLabV3+ (Xia et. al., 2021)	Based on DeepLabV3+ model	Trained on Cityscapes dataset, fine tuned with	Pixel-segmented

	proposed by Chen et. al., 2018)	GSV images collected by author.	GSV image
--	---------------------------------	---------------------------------	-----------

As the details of FCN-8 model are not included in the study, the accuracy measure is therefore not included in the accuracy comparison of models in Table 2.4.

Table 2.4 Accuracy comparison between both models

Model	Mean IOU (%)	Mean Absolute Error (%) compared with true GVI	Pearson Correlation Coefficient with true GVI	5-95% of GVI Estimation Error
Pixel Segmentation (Li et. al.)	44.7	10.1	0.708	-26.6, 18.7
DCNN semantic segmentation (Cai et. al., 2018)	61.3	7.83	0.830	-20.0, 12.37
DCNN end-to-end (Cai et. al., 2018)	NA	4.67	0.939	-10.9, 7.97
HRNet-OCR (Zhang and Hu, 2022)	80.6	NA	NA	NA
DeepLabV3+ (Xia et. al., 2021)	78.37	NA	NA	NA

According to the comparison of accuracies, we can see that HRNet-OCR (Zhang and Hu, 2022) has the highest mean IOU (%) and DCNN end-to-end model (Cai et. al., 2018) has the lowest mean absolute error compared with the true GVI. Nonetheless, due to the unavailability to retrieve HRNet-OCR model proposed, DeepLabV3+ model, the next best model in terms of mean IOU and DCNN are

developed and studied in this project.

#### **2.5.2.1 DCNN end-to-end model**

DCNN end-to-end model proposed by (Cai et. al., 2018) is based on a 50 layered deep residual network (ResNet) architecture (He et. al., 2015) by adding 3 more layers of dense connections at the end with the final layer consisting of a single sigmoid unit. Instead of the two-step process of pixel-wise segmentation of greeneries and GVI computation, this model is designed to directly estimate GVI as its output. Therefore, a sigmoid function is used for the final layer as the logistic regression function returns value between 0 and 1, which is the same range as the GVI.

To understand the deeper mechanism of this model, it is important to get know about the ResNet architecture. ResNet is a modified version of the plain convolutional neural network to deal with the degradation problem that is common amongst very deep neural network with many layers, i.e., the accuracy of network gets saturated with increasing depth and degrades rapidly beyond the saturation point. This impedes the improvements of model performance by adding more layers to the model. He et. al. suggests that the issue is caused by the solvers having difficulties in approximating identity mappings by multiple non-linear layers. This is because “if the added layers can be constructed as identity mappings, a deeper model should have training error no greater than its shallower counterpart”, which was proven not to be the case in their experiment.

ResNet architecture deals with the challenge by introducing shortcut connections that directly connecting the input data to the output of the stacked layers that acts as identity mapping that plain deep neural network has problem with. Formally, denoting the desired underlying mapping as  $H(x)$ , we let the stacked nonlinear layers fit the residual mapping of  $F(x) = H(x) - x$  instead of the desired mapping of  $H(x)$ . The original mapping is recast into  $F(x) + x$ . While both functions

asymptotically approximate the desired function, the residual mapping is easier to optimize as it is easier to just push  $F(x)$  to 0 in the case of identity mapping. The building block of residual learning is displayed in Figure 2.3, followed by a diagram displaying how ResNet works in Figure 2.4.

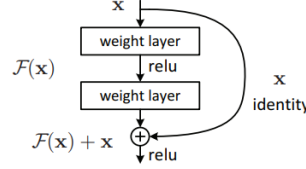


Figure 2.3 Building block of residual network.

source: [\[1512.03385\] Deep Residual Learning for Image Recognition \(arxiv.org\)](https://arxiv.org/abs/1512.03385)

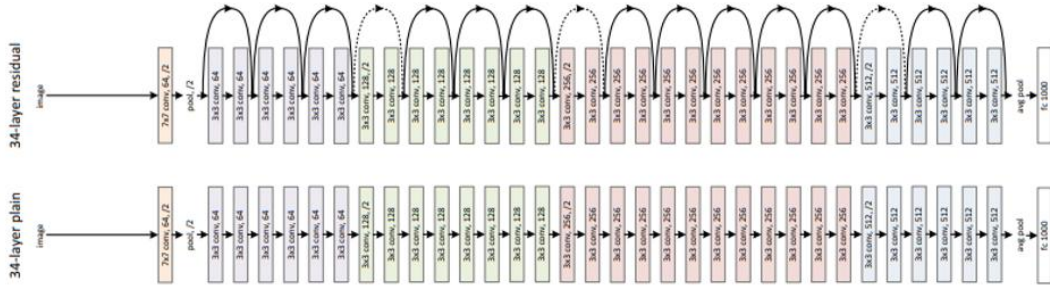


Figure 2.4 Residual network architecture diagram vs plain network.

source: [\[1512.03385\] Deep Residual Learning for Image Recognition \(arxiv.org\)](https://arxiv.org/abs/1512.03385)

Moving back to the discussion on DCNN end-to-end model, it has 28,138,601 parameters trained and fine-tuned with several datasets. The process of model training was first initialized with weights for ResNet that have been pretrained on the ImageNet dataset, then pre-trained with the transformed Cityscapes dataset and associated true GVI labels, and finally trained on small labelled GSV dataset collected by Cai et. al.

### 2.5.2.2 HRNet-OCR Model

High-Resolution Network-Object Contextual Representation (HRNet-OCR) is a stacked image segmentation model that combines HRNet and OCRNet used by Zhang et. al. in 2022 for GVI computation. The motivation for choosing such a

method for semantic segmentation is that the HRNet can be used to find out meaningful semantic features and the OCRNet explicitly transforms the pixel classification problem into an object region classification problem (Yuan et al., 2020).

*HRNet serves as the backbone of the model as the computation of GVI is a position-sensitive vision problem that can be improved significantly with high-resolution representations. Nevertheless, existing deep convolutional neural networks (DCNNs) frameworks are based on low-resolution representation subnetwork that is formed by connecting high-to-low resolution convolutions in series, and recover the high-resolution representation from the encoded low-resolution representation. Compared with DCNNs, HRNet improves the performance in position-sensitive image segmentation task by maintaining high-resolution representations through the whole process, allowing for a semantically richer and spatially more precise representation (Wang et. al., 2020). The improvements are enabled via two key characteristics: (i) Connect the high-to-low resolution convolution streams in parallel maintain the high resolution instead of recovering high resolution from low resolution, and accordingly the learned representation is potentially spatially more precise; (ii) Repeated fusions of representations from multi-resolution streams generate reliable high-resolution representations with strong position sensitivity. In short, HRNet achieves both complete semantic information and accurate location information by parallelizing multiple branches of the resolution, coupled with the constant interaction of information between different branches (Sun et al., 2019). The architecture of HRNet is illustrated in Figure 2.5.*

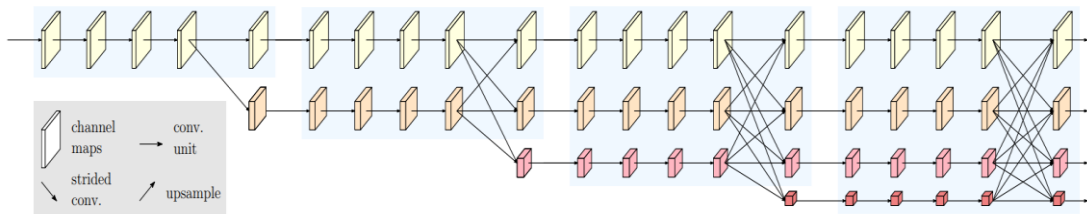


Figure 2.5 HRNet basic architecture diagram.

source: [1908.07919v2.pdf \(arxiv.org\)](https://arxiv.org/pdf/1908.07919v2.pdf)

Meanwhile, object contextual representation (OCR) is attached to the HRNet to enhance the performance of the image segmentation model. The main idea of

OCR is consistent with the original definition of the semantic segmentation problem, i.e. the class of each pixel is the class of the object to which the pixel belongs (Yuan et. al., 2021). In other words, OCR takes the context of each pixel into account when assigning a class label to it. In contrast with the previous relational context schemes that consider the contextual pixels separately and only exploit the relations between pixels and contextual pixels or predict the relations only from pixels without considering the regions, the proposed approach structures the contextual pixels into object regions and exploits the relations between pixels and object regions (Yuan et. al., 2021). By incorporating object information into the network, the resultant model can better capture the context of each pixel in the image and improve the accuracy of semantic segmentation.

On top of the HRNet backbone, the contextual pixels are divided into a set of soft object regions with each corresponding to a class, i.e., a coarse soft segmentation learned under the supervision of the ground-truth segmentation. The representation of each object region is then estimated by aggregating the representations of the pixels in the corresponding object region. Lastly, the representation of each pixel is augmented with the object-contextual representation (OCR), which is the weighted aggregation of all the object region representations with the weights calculated according to the relations between pixels and object regions.

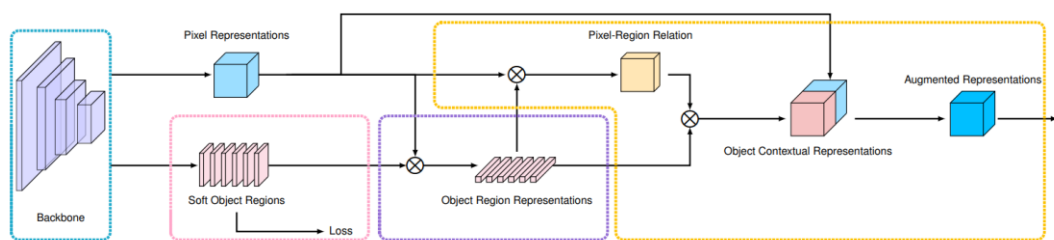


Figure 2.6 OCR basic architecture diagram.

source: <https://arxiv.org/pdf/1909.11065.pdf>

Zhang et. al. downloaded 5000 images with the correlated fine label in Europe open source labelled dataset Cityscapes to develop their segmentation model used for GVI calculation. The entire dataset is divided into train, validation, and test

sets with the ratio of 75:10:15 respectively.

### 2.5.2.3 DeepLabV3+ Model

DeepLabV3+ model is a deep learning model that integrates spatial pyramid pooling module in an encode-decoder structure used for image segmentation tasks, where the former extracts various levels of contextual information with pooling at different resolutions and the latter to find out sharp object boundaries (Chen et. al., 2018). This can be illustrated clearly in Figure 2.7.

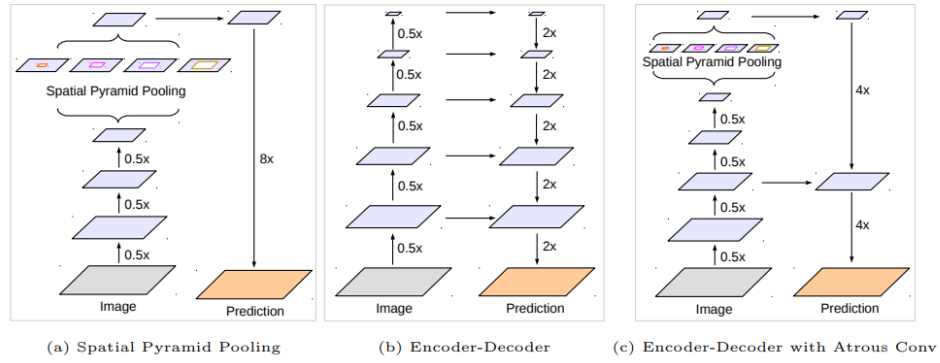


Figure 2.7 Components and basic architecture to develop DeepLabV3+ model.

Source: [1802.02611v3.pdf \(arxiv.org\)](https://arxiv.org/pdf/1802.02611v3.pdf)

Spatial Pyramid Pooling is pooling layers applied after the convolution layers to extract features at various resolutions to capture rich contextual features at different levels as shown in Figure 2.7 (a). Meanwhile, encode-decoder is made up of an encoder module that reduces the feature maps to extract semantic information and a decoder module that gradually up-samples the features as shown in Figure 2.7 (b). The combination of encoder and decoder forms a versatile structure that enables models to capture semantic information and make predictions accurately. On top of

On top of the integration of spatial pyramid pooling and the encode-decoder structure, atrous convolution, i.e. convolution layers with different dilation rates are used instead of conventional convolution layer to capture contextual information of multiple scales. The combination of components mentioned are illustrated in Figure 2.7 (c) to form DeepLabV3+ architecture.

## 2.6 Performance Measure for GVI Prediction

Cai et. al. (2018) proposed two metrics to evaluate the performance of tree cover estimation, i.e. mean Intersection over Union (IOU) to measure the accuracy of the location of labeled greeneries pixels, and mean absolute error (MAE) for the accuracy of overall GVI.

In computer vision, the mean IOU is commonly used for object detection and segmentation. It is defined as the ratio between the area where predicted objects or pixels overlap with the target object over the area of the union of both (Padilla et. al.), see Figure 2.8. In the context of GVI computation, the predicted and target values are both the pixels consisting of greeneries in the street view images.

$$IOU = \frac{\text{area of overlap}}{\text{area of union}} = \frac{\text{Figure 2.8 Illustration of the intersection over union (IOU)}}$$

Figure 2.8 Illustration of the intersection over union (IOU)

Source:

[https://www.researchgate.net/publication/343194514\\_A\\_Survey\\_on\\_Performance\\_Metrics\\_for\\_Object-Detection\\_Algorithms](https://www.researchgate.net/publication/343194514_A_Survey_on_Performance_Metrics_for_Object-Detection_Algorithms)

The IOU of greeneries pixels can be calculated with formula shown in Equation (2.2).  $n$  is the number of images in test data,  $TP_i$  refers to true positive predicted greeneries label in image  $i$ ,  $FP_i$  refers to the false positive predicted greeneries label in image  $i$ ,  $FN_i$  refers to the false negative predicted greeneries label in image  $i$ .



$$IoU = \frac{1}{n} * \sum_{i=1}^n \frac{TP_i}{TP_i + FP_i + FP_i} \quad (2.2)$$

Equation (2.1) shows the formula to calculate IOU.

As for the accuracy of GVI value, it can be measured with the usual evaluation metrics used in regression. For instance, root mean square error (RMSE) proposed and mean absolute error (MAE) by (Dong et. al., 2018) and (Cai et. al., 2018) respectively. A model with the lowest MAE or RMSE has the highest accuracy. Their formulas are as shown below as Equation (2.3), Equation (2.4).  $\hat{y}_i$  refers to the predicted label of a pixel,  $y_i$  refers to the true label of a pixel. M refers to the number of pixels in a GSV image, n refers to the number of images in test set.

$$RMSE_j = \sqrt{\sum_{i=1}^M \frac{(\hat{y}_i - y_i)^2}{M}}, \quad \overline{RMSE} = \frac{1}{n} \sum_{j=1}^n RMSE_j \quad (2.3)$$

Equation (2.3) shows the equation to calculate RMSE.

$$MAE_j = \frac{1}{M} \sum_{i=1}^M |y_i - \hat{y}_i|, \quad \overline{MAE} = \frac{1}{n} \sum_{j=1}^n |MAE_j| \quad (2.4)$$

Equation (2.4) shows the equation to calculate MAE.

Other than measuring the accuracy of prediction, Pearson correlation coefficient ( r ) is used to evaluate whether the predicted GVI can accurately model the underlying patterns in the true GVI. The calculation of Pearson correlation coefficient is demonstrated in Equation (2.5), where r is the correlation coefficient,  $x_i$  is the predicted GVI value for image i,  $\bar{x}$  is the mean predicted GVI,  $y_i$  is the true GVI for image i,  $\bar{y}$  is the mean true GVI.

$$r = \frac{\sum (x_i - \bar{x})(y_i - \bar{y})}{\sqrt{\sum (x_i - \bar{x})^2 \sum (y_i - \bar{y})^2}}$$

(2.5)

Equation (2.5) shows the formula to calculate Pearson correlation coefficient (  $r$  ).

Finally, there is another metric used to evaluate the variance and distribution of the difference between predicted and true GVI, that is 5-95% Estimation Error. For this metric, closer the central value is to 0 and smaller the range of the value is deemed to be better performing.

## 2.7 Interpretation of GVI

GVI is defined to be the green view that one can see at a single point, typically on a street level. By combining the GVI extracted from many sampling points, one can connect the dots and come up with a comprehensive plot of the visibility of urban greeneries in the studied site. For instance, the Treepedia project by the MIT Senseable City Lab is mapping GVI across many major cities in the world to explore their green distributions as shown in Figure 2.9.



Figure 2.9 Map plots of GVI for Amsterdam and Singapore as an illustration.

Source: [Treepedia :: MIT Senseable City Lab](https://treepedia.mit.edu/)

Other than directly mapping GVI on streets, the data can also be aggregated at an area-level by mean or median to ease the extraction of meaningful information by stakeholders such as planners and local governments. Nevertheless, there is a big potential to bias if the GVI is simply aggregated by the mean of points per area due

to the difference in density of data collection. Kumakoshi et. al. (2020) modified the GVI calculation to propose a Standardized Green View Index (sGVI) as a weighted aggregation of GVI scores in a study area. The formula is shown in Equation (2.6).  $i$  represents the point of GVI calculation, while  $l_i$  represents the total length of links (streets) that the point  $i$  is associated with, and  $l$  is the total length of all links in the zone.

$$sGVI = \sum_{i=1}^n GVI_i * \frac{l_i}{l} \quad (2.6)$$

Equation (2.6) shows the formula to calculate sGVI.

On top of the mapping of GVI or sGVI values on map, multiple secondary data such as the width of road (Dong et. al., 2018), ethnic distribution (Li et. al., 2015) can also be used to investigate the effects or reasons behind differences in GVI.

## 2.8 Issues

Overall, there are multiple issues that can be identified from the literature review. To the best of our knowledge, there are no GVI studies in Malaysia, resulting in a missing potential to measure urban greeneries coverage from the users' perspectives. As the computation of GVI was labor intensive (manual selection of greeneries), it is important that we choose an effective method to automate the extraction of greeneries from the street view images. In the literature review, we have come across multiple methods such as Pixel Segmentation (Li et. al. 2015) and deep learning models (Cai et. al., 2018) based on convolutional neural networks (CNN) such as PSNet and ResNet that were used by previous researchers for the task. It is important that we explore these methods and choose the most accurate and interpretable model to compute our GVI. Finally, it is also essential that we can

visualise the computed GVI so that they can be interpreted effectively in meaningful ways to assist spatial planning of the cities.

## **CHAPTER 3**

### **RESEARCH METHODOLOGY**

#### **3.1 Research Framework**

The aim of this project is to visualize the state of urban green coverage in Malaysian city from the users' perspective with Green View Index (GVI). To achieve the aim, the research project is broken down into several phases that form the research framework.

In Phase 1, problem formulation is carried out to set up the foundation for research. It starts by determining the field of interest and the topic to continue research. It is then followed by literature review where the current state of research is analysed to form background understanding on the research topic and discover research gap. After that, the aim and objectives of the research is formulated and consolidated along with the defined scope of study area, which in this case being referred to the Johor Bahru city center.

After problem formulation, Phase 2 of data preparation is carried out at the beginning of the research project. In the preparation step, data is first collected, then pre-processed according to the need of the research. In the context of this research, the collected image data is converted into RGB format and masked to generate ground truth data for supervised learning.

Subsequently, the prepared data is used for models' development and evaluation in Phase 3. In this phase, Pixel Segmentation model is developed as the benchmark model to compare with the deep learning models developed to predict GVI in terms of accuracy. Finally, the predicted results are used for reporting and EDA in Phase 4. The generated insights are then presented on a dashboard as the final product.

The summarised diagram that displays the research framework is displayed in Figure 3.1 below.

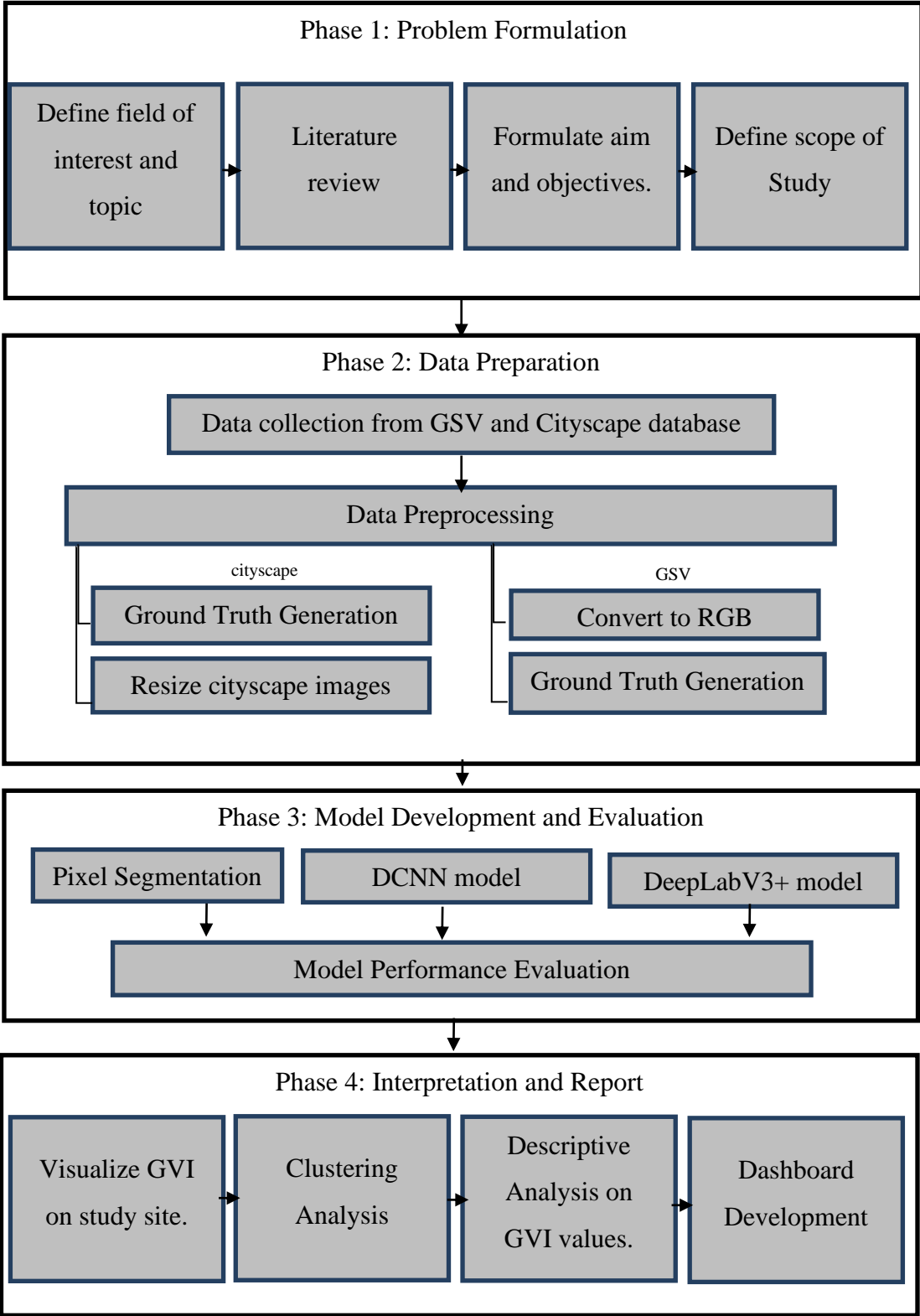


Figure 3.1 Project research framework

## **3.2 Data Preparation**

To compute Green View Index (GVI) in target site, street view images in Johor Bahru City Center are needed. The data preparation for the project can be broken down into 2 parts, i.e. (1) sampling and retrieving street view data and (2) image preprocessing.

Besides, another set of street view data is collected from an open source dataset, Cityscape is also used to augment GSV collected from Johor Bahru City Center to improve the accuracy of model.

### **3.2.1 Data Collection**

#### **3.2.1.1 Sampling Street View Data**

To limit the scope and resources required for the project in a manageable range, the methods used sampling of data collection points are improvised to fit within the Google Street View API framework. The image sampling processes are carried out in several steps:

##### **1. Decide on the study site and its boundary.**

The city center of Johor Bahru is selected as the study site as it has a high level of activity, movement and population density, making it a good representation of a Malaysian city suitable for our study. Due to the lack of official boundaries demarcating the Johor Bahru city center area, an expedient demarcation is made by using *Jalan Lingkaran Dalam* (dashed line) as an edge.

In order to retrieve street views from Google Street View using coordinates, the study site boundary has been defined as a circle with a radius of 1000m centered on the coordinates of Komtar JBCC. This boundary has been chosen based on several trials to ensure that it covers the busiest part of Johor Bahru city center. The boundary of the study site is illustrated in Figure 3.2 below.

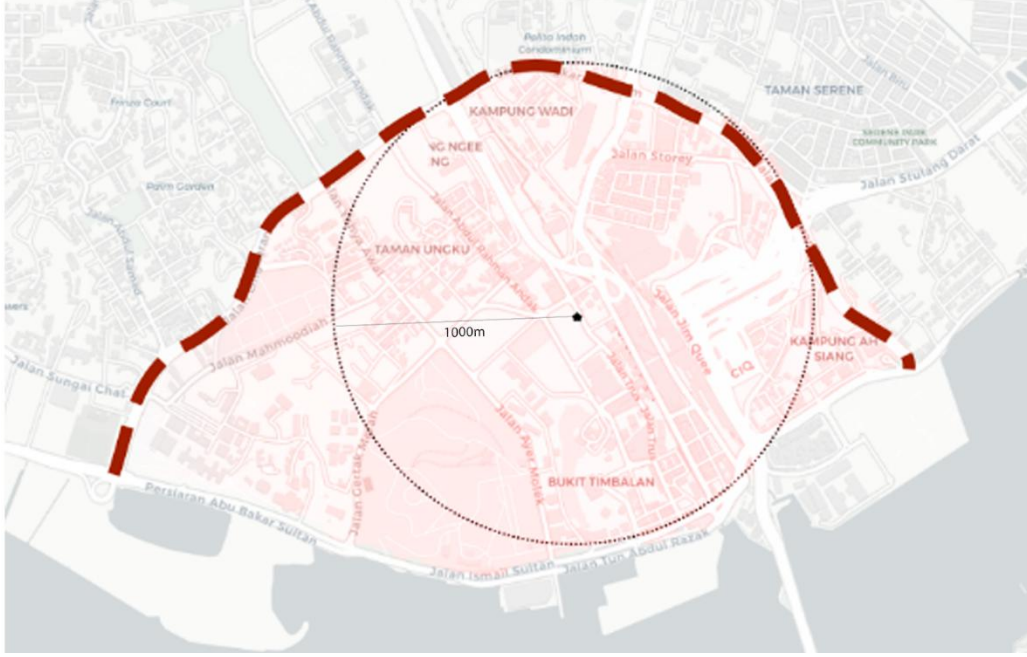


**Figure 3.2** Study site plan with boundaries.

## **2. Sampling random coordinates on streets within the boundary.**

The random coordinates are defined by using Pythagoras theorem, following Equation (3.1) to ensure that they are located within the 1000m circular boundary. The center latitude and center longitude represent the latitude and longitude of the center of study site, Komtar JBCC; latitude and longitude represent any random coordinate generated. The radius of the site boundary is converted to degrees of latitude at the equator by dividing it by the approximate distance of 111km per degree of latitude.

$$latitude \leq center\ latitude \pm \sqrt{radius^2 - (longitude - center\ longitude)^2} \quad (3.1)$$

Equation (3.1) shows the formula used to limit random sample points within 1000m radius from the center coordinates (*Komtar JBCC*).

## **3. Retrieve GSV images from the sampled coordinates.**



Various GSV parameters discussed in the literature review, e.g. GVI4, GVI, GVI8, GVI16 are explored from the perspectives of zoom, distortion, overlap of images and cost to find out the best configuration to use for our task of GVI computation. The value for each parameter is determined in place in the following sequence.

- i. **Field of view.** The field of view of GSV images are set to the minimum of 65 to minimize the proportion of noise included in images collected, e.g. road and sky that are not typically in our field of focused vision unless special attention is given to.
- ii. **Headings.** Based on the field of view used, the headings of visuals decide the images retrieved from a single location excluded parts of the view or overlapped with one another. With trial and error, 6 pictures facing different directions of 0°, 60°, 120°, 180°, 240°, 300° to capture every view that one might see while minimizing overlap as illustrated in Figure 3.3.
- iii. **Pitch.** A slight pitch of 10 degree upwards is applied to reduce the proportion of road being captured in the image.

The parameters set is shown as follows, with a for loop used to take multiple images of different headings.

```
params = {  
    'key': api_key,  
    'size': '1280x1280',  
    'fov': 65,  
    'location': f'{latitude},{longitude}',  
    'heading': 0,  
    'pitch': 10  
}
```



**Figure 3.3** Sample view collected from a sample point at (1.4574946, 103.7690224)

In total, 6385 images from 1065 sample locations were selected. The street view images are saved as RGB format and their metadata, latitude, longitude and heading are stored as a csv file for possible future use. Table 3.1 displays the first few rows of metadata. The selected sample locations are plotted on a map (Figure 3.4) to visualize the density of sampling.

Table 3.1 The metadata of sampled images.

	lat	Lng	heading
0	1.46143	103.7624	300
1	1.461554	103.7623	0
2	1.461554	103.7623	60

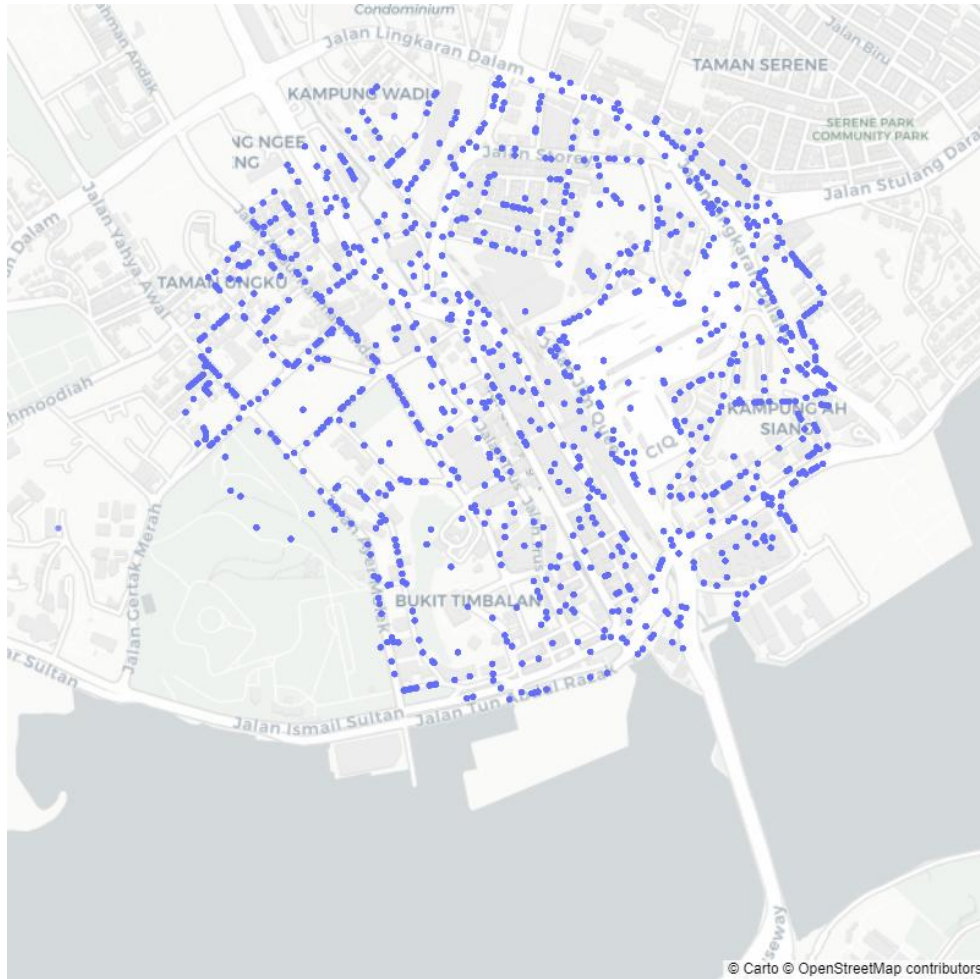


Figure 3.4 Map plot of sampled locations

### 3.2.1.2 Cityscape Data Collection

Cityscape dataset is downloaded from <https://www.cityscapes-dataset.com/downloads/>. From the site, two zip files: *gtFine\_trainvaltest.zip* (241MB) [md5] consisting of segmented street views labelled data and *leftImg8bit\_trainvaltest.zip* (11GB) [md5] consisting of street view images are downloaded. Both zip files have complementary image pairs in train (2975 images), val (500 images), test folders (1525 images) respectively. Nevertheless, it is worth noting that the test folder in the segmented street view labelled data are null sets that cannot be used.

The dataset segmentation consists of 30 label classes. In the data processing section, 30 label classes are to be converted to only 2 classes of green view or non-green view. Figure 3.5 shows an example of how Cityscape dataset's street view image and its complementary looks.



Figure 3.5 The street view image and its complementary segmentation label image from Cityscape dataset.

### **3.2.2 Data Preprocessing**

#### **3.2.2.1 Data Pre-processing for GSV**

To develop a deep learning model, labeled data is needed. In this case, the data for model development consists of images and the labels correspond to the presence or absence of vegetation in those images. There are two types of labeled data needed:

1. Extract vegetation pixels from the images. To create the labels, binary masks are applied to the images, where vegetation is represented by white pixels and all other areas are represented by black pixels. This helps to simplify the images and make the training process more efficient. A sample is shown in Figure 3.6.



**Figure 3.6** A sample of the street view image and its target mask.

2. GVI at every sample point used for model development. To develop models that can accurately predict GVI, GVI calculated from the manually extracted vegetation pixels are used as the ground-truth. GVI is calculated with Equation (3.2).

$$GVI = \frac{\sum_{i=1}^n \sum_{j=1}^M Area_g}{\sum_{i=1}^n \sum_{j=1}^M Area_t} \quad (3.2)$$

Equation (3.2) shows the formula to calculate GVI.

At the end of the data preprocessing, input data for model development is prepared: street view images represented in *Numpy* array format (training data), the true GVI of each street view image used for training and testing (target data).

### 3.2.2.2 Data Pre-processing for Cityscape Data

The preprocessing for cityscape data can be broken down into steps below:

Firstly, load all training data and validation data from *gtFine\_trainvaltest.zip* (241MB) [md5] (segmented street views labelled data) and

*leftImg8bit\_trainvaltest.zip* (11GB) [md5] (street view images) as *NumPy* array. Then, transform the array into RGB format by extracting only the first 3 channels. Both resulted *NumPy* arrays should have the shape of (number\_of\_images, height, width, number\_of\_channels), which in this case are (number\_of\_images, 512, 1024, 3) and (number\_of\_images, 512, 1024, 3).

To appropriate cityscape data for GVI computation, a change of the multiclass segmentation into binary segmentation of green view and non-green view is needed. It is done by determining the unique colours in the label images, then change values of the colour pixels with labels representing green view ('vegetation' and 'terrain') to [1,1,1] and other pixels to [0,0,0]. The generated binary segmentation data is then converted into array with only 1 channel with shape (number\_of\_images, 512, 1024) to save memory and makes GVI computation more convenient.

Finally, the arrays representing street view images and binary label data is clipped into a square shape of size (512, 512) so that it has the same square layout as the GSV images. GVI of the images are generated as the ground truth by summing up the values in the binary label data array divide by (512\*512).

### 3.2.3 Splitting Data for Model Development

In the *Treepedia* study published by Cai et. al, 320, 80, and 100 google street view images are used for training, validation and testing respectively. This serves as a benchmark for the number of images used for model training in this project. As the model deployed was published on github: billcai/treepedia\_dl\_public: Treepedia 2.0: Deep Learning Based Large Scale Quantification of Urban Canopy Cover (github.com), we can use transfer learning to train the model for the project with relatively fewer data.

Thus, in this project, a slightly lower number, 280 GSV images are used for training to reduce the training time, while 80 and 80 images are used for validation and testing respectively due to the large amount of time needed for manual data labelling for ground truth generation.

As for the cityscape dataset, 2975 images are used for training and 500 are used for validation. As it is only used for model pretraining, test data is not required.

### **3.3 Model Development for GVI Prediction**

In this project, the classical Pixel Segmentation method proposed by Li et. al., 2017 is benchmarked against two supervised deep learning models DCNN end-to-end model and DeepLabV3+ model.

The Pixel Segmentation model is used as the benchmark as it is the most widely adopted approach used to compute GVI of street view images. Besides, compared with supervised deep learning models, the Pixel Segmentation approach comes with several major benefits, e.g. greater interpretability, less susceptible to human induced error in the data preprocessing stage, no need of time and computation resources for model training.

Due to the benefits mentioned above, deep learning models need to predict GVI with higher accuracies to show that they worth more than what they cost.

#### **3.3.1 Pixel Segmentation Method**

Firstly, separate bands of red, green and blue are extracted from the RGB images. As we wish to find pixels that have higher green band values than the other two bands, differences are computed by subtracting the red band and blue band from

the green band respectively. If both differences are larger than 0, they are multiplied to form a new Difference image. The generated Difference image is a grayscale mask that represents the number of differences between the green band of a pixel with the other two bands. The lighter the pixel or the higher its value, the ‘greener’ the pixel appears in the original picture and vice versa.

To eliminate noise, a threshold is assigned such that selected pixels with value larger than threshold are assigned to value of 255 and those below assigned 0. The outcome classifies the selected pixels as vegetation, while the others as not vegetation. After this, the GVI of an image can be easily computed from the classification outcome with Equation (3.2). Figure 3.7 simplifies and illustrates the whole process.



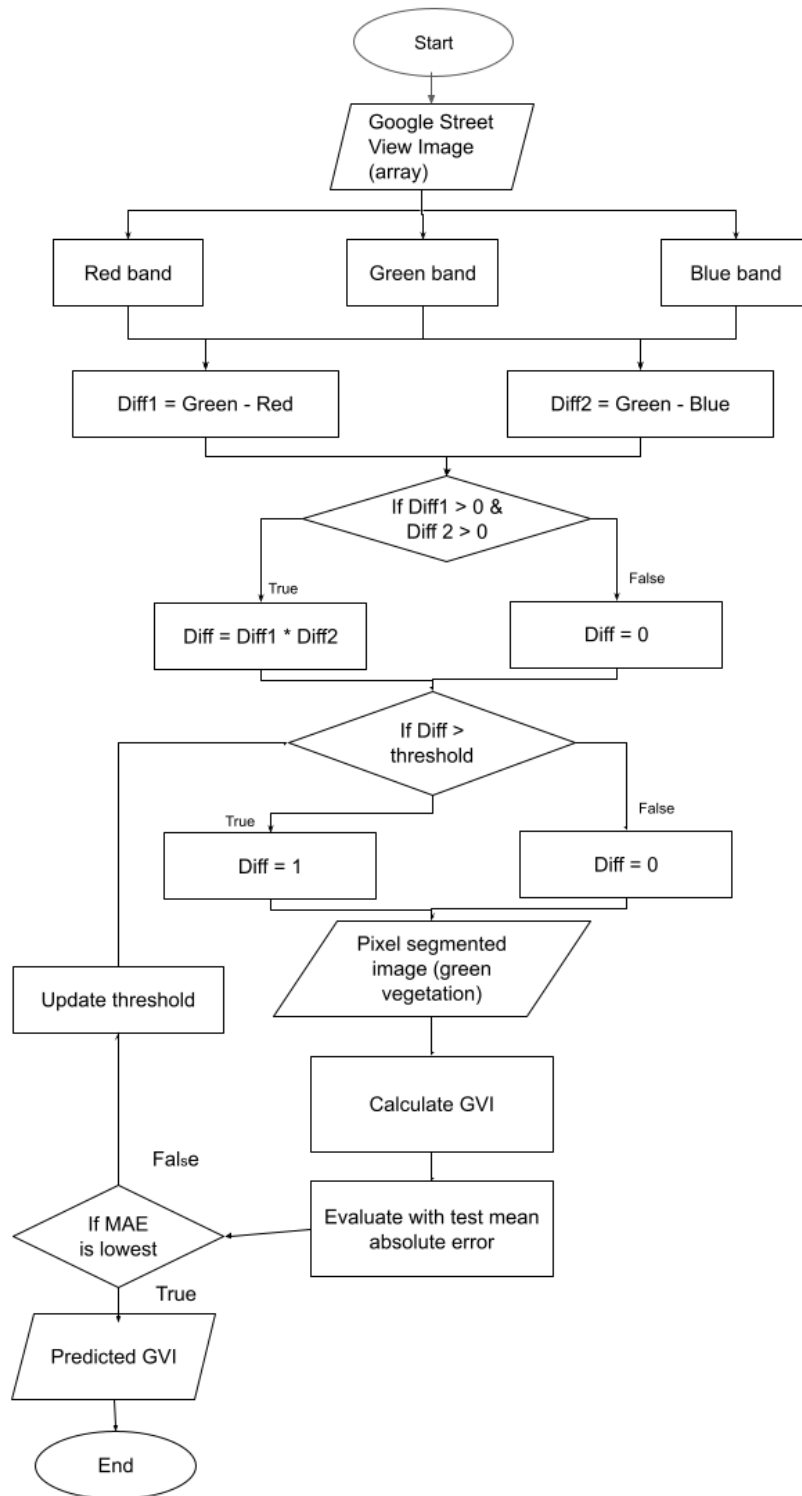


**Figure 3.7** The process of Pixel Segmentation for green vegetation extraction and GVI calculation.

### 3.3.2 Deep Learning Models

Deep learning models developed and studied in this project are supposed to be the models shown to have the highest performance in the literature review, i.e. DCNN end-to-end model with mean absolute error of 4.67% and HRNet-OCR with mean IOU of 80.6%. Nevertheless, due to the issues and complexity to retrieve HRNet-OCR model from the suggested repository, the DeepLabV3+ model with the mean IOU of 78.37% is used to predict GVI.

The DCNN end-to-end model is downloaded from the Github repository uploaded by Cai: billcai/treepedia\_dl\_public: Treepedia 2.0: Deep Learning Based Large-Scale Quantification of Urban Canopy Cover (github.com), while DeepLabV3+ structure is set up with code provided by Tensorflow keras site: [https://keras.io/examples/vision/deeplabv3\\_plus/](https://keras.io/examples/vision/deeplabv3_plus/). Nonetheless, as the output of DeepLabV3+ model is pixel-segmented image which is different from that of GVI prediction generated from DCNN end-to-end model, several Dense layers are connected to the output of DeepLabV3+ model, with the last layer of neuron having a sigmoid function as activation function to change the output to GVI values between 0 and 1 so that both deep learning models can be compared on the same level.

The trained DCNN model was pre-trained on ImageNet dataset, then trained on Cityscapes dataset, and finally on 320 GSV images collected by Cai et. al. For DeepLabV3+ model, pretrained ResNet50 retrieved from Keras is used as the backbone of its encoder module and trained on the preprocessed cityscape data. Then transfer learning is done on both pre-trained models (DCNN end-to-end and DeepLabV3+ model) by fine-tuning it based on local street view images collected. The trained model is then used to directly predict the GVI values of GSV images. Figure 3.8 showcases the process to develop deep learning models to predict GVI in this project.

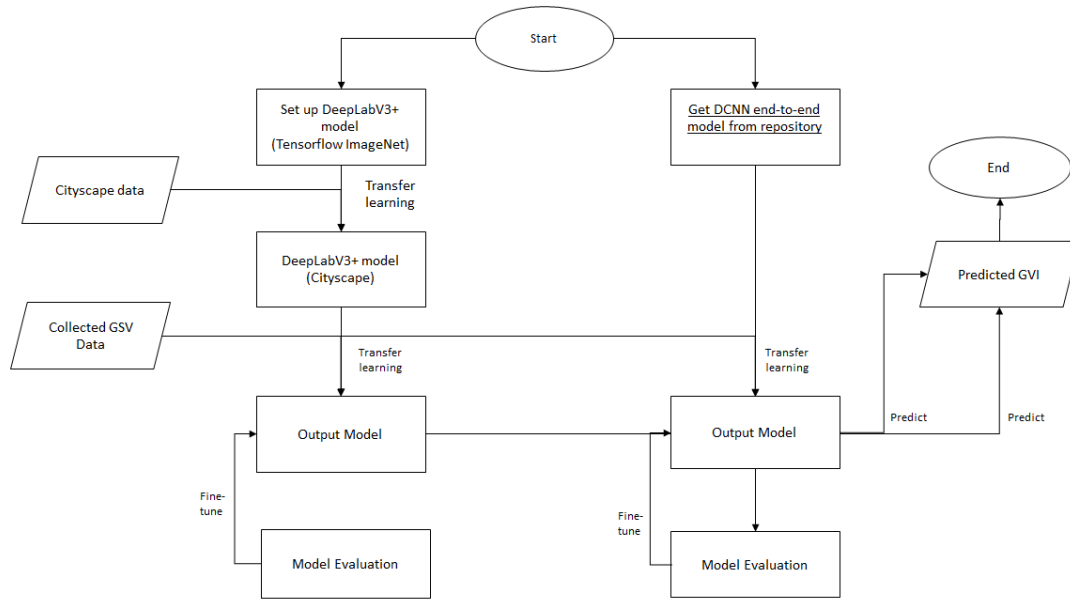


**Figure 3.8** The process to develop deep learning models to predict GVI.

In the case of deep learning model training at each step of model fine tuning, hyperparameter tuning plays an important role. For each model, a set of hyperparameters are tuned.

- DCNN end-to-end model: learning\_rate = [0.0001, 0.001, 0.01],  
batch\_size = [16, 32, 64]
- DeepLabV3+ model : learning\_rate = [0.0001, 0.001, 0.01], batch\_size =  
[8, 16, 32], number of trainable layers = [4, 8, 12]

RandomSearch method in Keras-tuner package is used to automate the search of best hyperparameters for each model training. Nonetheless, due to memory limitations, manual fine tuning is also required in most cases.

### 3.3.3 Evaluation of Models

The final outputs of the models are all predicted GVI values between 0 and 1. The accuracy of the prediction models are defined by its error rate: the lower its error rate, the higher its accuracy. With the 80 images from test data, following the metrics

used by studies covered in Chapter 2, mean absolute error (MAE) in percentage, 5-95 percentile of MAE, Pearson correlation coefficient with the true GVI values ( $r$ ), are used as the parameters to assess the error rates of the proposed prediction models. Smaller values for MAE and  $r$  value closer to 1 represents higher accuracy. Meanwhile, 5-95 percentile of MAE is used to measure the centrality and spread of the error. For this metric, the desired outcome is for the spread to be small and centered on 0.

Other than accuracy, it is also important to find out underlying biasness in models. Thus, bias analysis for models is carried out by plotting error (prediction – true GVI) against the predicted GVI values. This allow us to look into the bias of the models at different levels of GVI. Besides, the frequency of underestimation and overestimation at different predicted GVI levels are documented and discussed as well.

Other than accuracy, the models are also evaluated by the inference time. The time taken to predict 1000 GVI values for each model is recorded.

### **3.4 Dashboard and Report**

The results generated from the GVI predictions are used to understand how often the people in the site can view greens in their daily lives. Thus, further exploratory analysis on the patterns underlying distribution of GVI predictions in Johor Bahru city center is carried out. Moreover, a dashboard is built to provide an interface to the findings of this project.

### **3.4.1 Clustering Analysis**

Clustering analysis is essential to help us to figure out the underlying patterns of GVI distribution in the site. Nonetheless, it is no trivial task to know which clustering method to apply on the GVI predictions on site. In this case, there are several parameters to experiment with to find out the best clustering approach:

1. Clustering model: partition-based clustering (Kmeans) and hierarchical clustering (agglomerative clustering)
2. Number of clusters

The clustering results are evaluated based on both silhouette score and inertia to find out the best approach to clustering.

Exploratory data analysis is carried out on each cluster generated to find out the characteristics of each cluster and thereby probable solutions that can improve GVI in the target site.

### **3.4.2 Dashboard Development**

The dashboard provides a user-friendly interface to access the findings from the project. The developed dashboard should include 2 main components:

1. Allow the user to gain understanding on the prediction models developed for GVI prediction. This makes sure that the users of the dashboard are informed about the underlying bias and errors that might present in the prediction results.
2. Allow users to learn about the GVI distribution and their underlying patterns on site easily.



## CHAPTER 4

### RESULTS AND DISCUSSION

#### 4.1 Performance of Models in GVI Computation

With the 80 samples used for testing, the models are evaluated for their accuracy, robustness, and inference time. Table 4.1 records the evaluation results for each model.

**Table 4.1** Evaluation of performances of different models for GVI computation.

Model	Mean Absolute Error (%)	Pearson Correlation Coefficient with true GVI ( r )	5-95% of GVI Estimation Error	Inference time (seconds per 1000 data)
Pixel Segmentation model	6.7772	0.944534	( -0.065886, 0.198102)	9.99
DCNN end-to-end	4.5872	0.969098	( -0.067116, 0.087973)	43.87
DeepLabV3+ end-to-end	6.7139	0.924098	( -0.138696, 0.143834)	121.83

#### 4.1.1 Accuracy Evaluation

According to the observations above, the DCNN end-to-end model have the highest accuracy out of the 3 models with the lowest mean absolute error at 4.58% and the highest Pearson correlation coefficient with the true GVI at 0.97 compared with that of 6.78%, 0.94 for the Pixel Segmentation model and 6.71%, 0.92, for the DeepLabV3+ model. Meanwhile, though DeepLabV3+ model has a slightly lower mean absolute error than the Pixel Segmentation model, it has a lower correlation coefficient with the true GVI compared with the Pixel Segmentation model. This shows that while DeepLabV3+ to be slightly worse off than the Pixel Segmentation method in capturing the patterns of the true GVI distribution.

#### 4.1.2 Robustness Evaluation

The robustness of models is evaluated with 5-95% of GVI estimation error. In this case, the DCNN end-to-end model still shows the greatest performance with the smallest range of 5-95% GVI estimation error at 0.16 (-0.067116, 0.087973). This is much smaller than that of DeepLabV3+ and Pixel Segmentation models, with ranges of 0.28 (-0.138696, 0.143834) and 0.31 (-0.018923, 0.303153). The GVI estimation error is further explored with the charts in Figure 4.1 to understand the patterns of GVI prediction errors for each model. Constant line 0.075 is the mean absolute error of GVI for all 3 models while the other constant line in each chart is the mean absolute error for their respective models. X-axis is represented by grouped bins of GVI prediction with bin size of 0.05, while y-axis is represented by the mean absolute error of each bin.



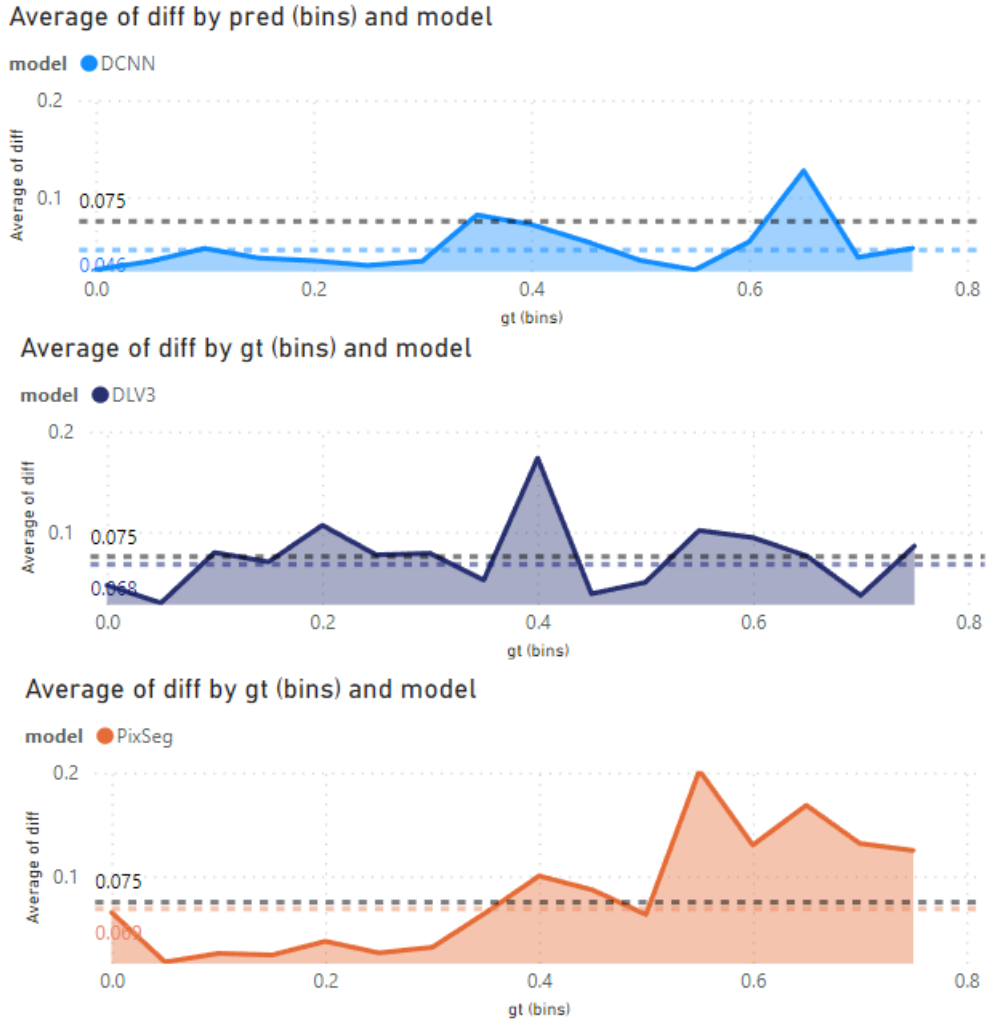


Figure 4.1 GVI prediction error for the 3 models studied.

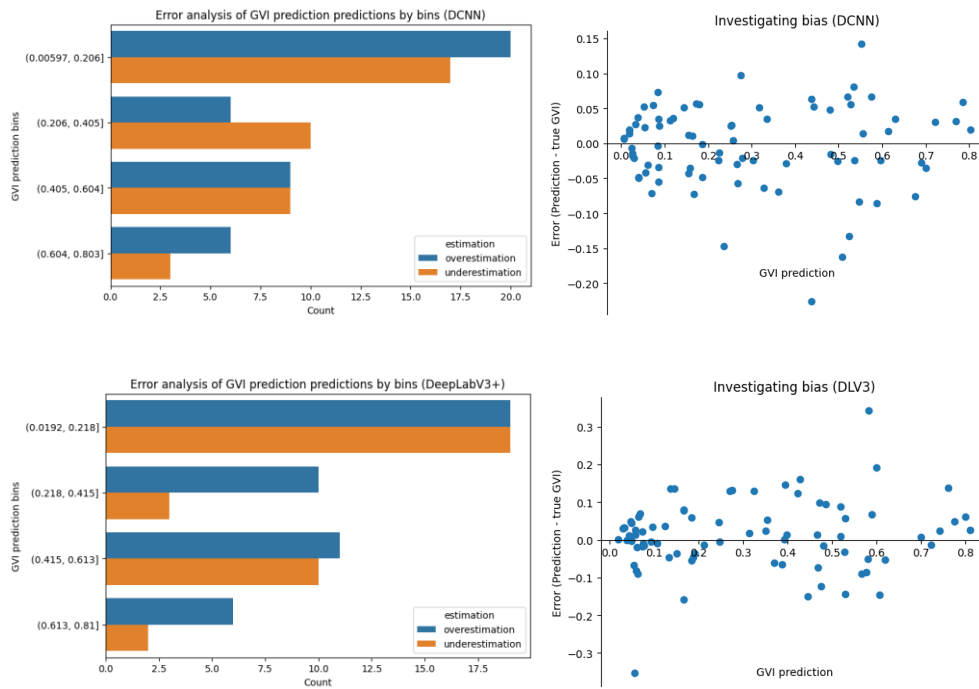
In Figure 4.1, we can observe that the mean absolute error for DCNN predictions is consistently lower than the mean absolute error of all 3 models across various prediction bins. This is followed by the DeepLabV3+ model and the Pixel Segmentation model with similar mean absolute error at 0.068 and 0.069 respectively. Both have a different distribution where DLV3+ have the consistent error across prediction bins while Pixel Segmentation model has a very low error at lower predicted GVI but higher error with higher predicted GVI values.

### 4.1.3 Inference Time Evaluation

Unsurprisingly, the Pixel Segmentation model has the shortest inference time out of the 3 models with only 9.99s needed to predict 1000 GVI values due to the simplicity of its algorithm. It is followed by the DCNN model that can predict 1000 GVI values with 43.87s, and lastly DeepLabV3+ with 121.83s.

### 4.1.4 Bias Analysis for Prediction Models

The underlying bias of the models should be investigated to allow more interpretable prediction results for the users. In this case, the underlying bias of the models are studied by looking into how often the models underestimate and overestimate, and the distribution of the differences caused by it in Figure 4.2



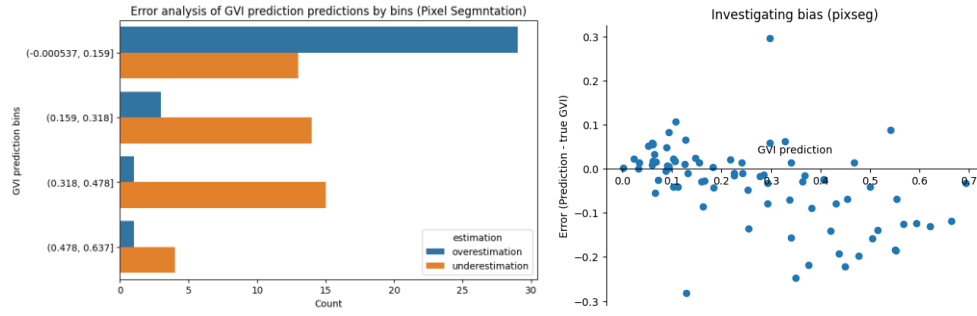


Figure 4.2 The frequency of underestimation and overestimation of model and bias investigation for 3 models.

In the charts above, it is observed that the DCNN model is relatively unbiased and DeepLabV3+ models are slightly positively biased by overestimating more than underestimating (46 vs 34). In the case of Pixel Segmentation model, it is negatively biased with 46 underestimations out of 80 testing data, with a very clear negative bias as shown in its error over GVI prediction chart.

## 4.2 Visualization of GVI Prediction in Study Site

Based on the model with higher accuracy, the predicted GVI values within the study site are visualized to allow further analysis on its urban vegetation coverage. In Figure 4.3, the mean GVI predictions at each one of the 1002 spots calculated by the mean GVI prediction at each single point where images are taken are visualized on a map plot. Red scatter plots represent spots with low GVI while green plots represent high GVI values. The distribution of predicted GVI are shown in the histogram on the right side of the dashboard, with purple dotted line representing its median and blue dotted line representing its mean.

## Visualisation of GVI Prediction on Site



Figure 4.2 Dashboard visualising the GVI predictions on target site.

Based on Figure 4.1, there are several vague patterns discovered in the distribution of GVI values. For instance, the East side of the study site appears to have lower GVI values than the West; the South-East part of the site has the highest density of red points with low GVI. These observations suggest that GVI values in the study site vary due to their locations. To investigate the reasons contributing to the differences, clustering analysis is carried out in Chapter 4.4.

Due to the differences in each model the distribution of GVI predictions of 3 models are significantly different from one another. This can be observed from the histograms displayed in Figure 4.3.

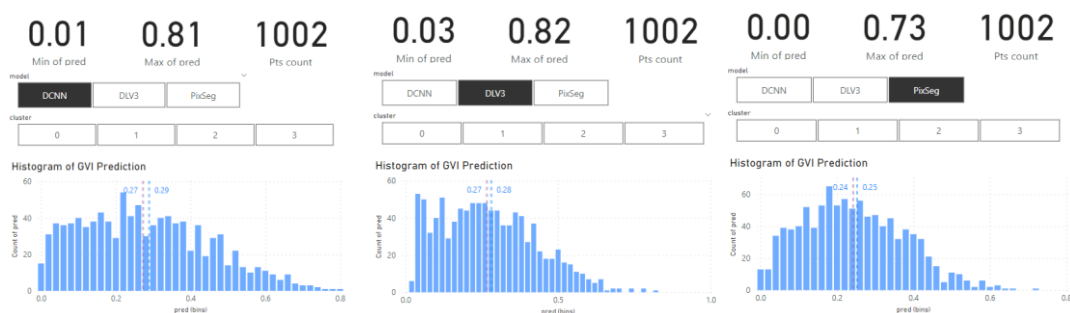


Figure 4.3 Distributions of GVI predictions with 3 different models.

For DCNN model, its GVI predictions have a unimodal, positive skew and a broad spread. It consists of a range from 0.01 to 0.81 for its predicted GVI. For

SeepLavV3+ model, it has a unimodal, positive skew distribution for its GVI predictions. While it has a similar range with DCNN's prediction (0.03 to 0.82), its predictions have a slightly narrower spread compared with DCNN model's predictions.

As for the Pixel Segmentation model, it has a significantly more normal distribution compared with the other two as there is a shorter right tail. It has a smaller range of only 0.00 to 0.73.

### 4.3 Clustering Analysis of GVI

Both partition-based clustering and hierarchical clustering are carried out for all 3 models' GVI predictions (DCNN, DeepLavV3+, Pixel Segmentation) to determine the best clustering approach. As the location of sampling is an important part of the analysis, the latitude and longitude of sample points are included in the clustering analysis as well.

For partition-based clustering (Kmeans) and hierarchical clustering (agglomerative clustering), the number of clusters needs to be predetermined based on the insights that we are extracting and how well one cluster differentiates from another. In this project, the latter is informed by utilizing silhouette score. Therefore, in Figure 4.4 and 4.5, silhouette score is plotted against the number of clusters for both clustering approaches applied on different models' predictions.

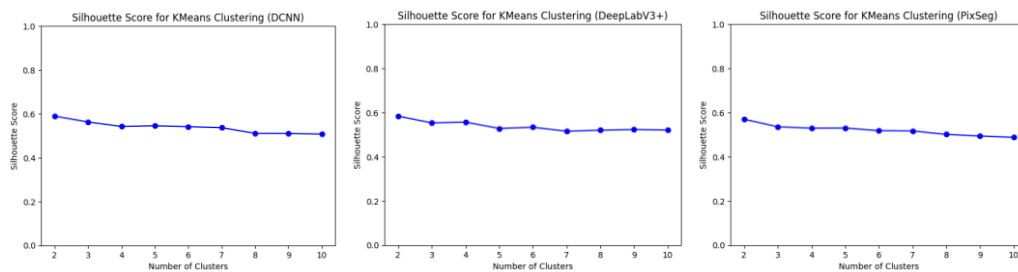


Figure 4.4 Kmeans clustering for GVI predictions based on DCNN, DeepLabV3+ and Pixel Segmentation model.

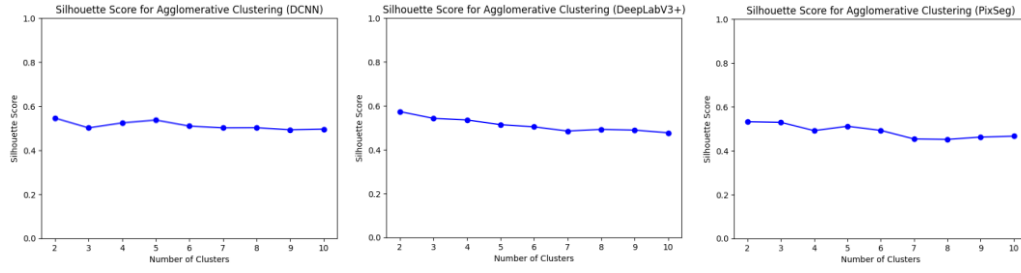


Figure 4.5 Agglomerative clustering for GVI predictions based on DCNN, DeepLabV3+ and Pixel Segmentation model.

In Figure 4.4 and Figure 4.5, we also notice that Kmeans has a slightly higher silhouette score compared to that of agglomerative clustering across all number of clusters tested. Thus, Kmeans is selected as the method for clustering analysis. To ensure that Kmeans is suitable for the dataset, latitude, longitude and mean GVI prediction per sample spot is plotted in a 3D scatterplot to ensure the data distribution is spherical in Figure 4.6.

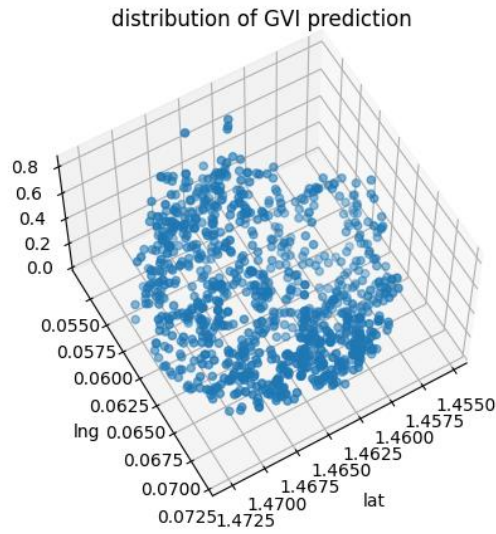


Figure 4.6 Scatterplot latitude, longitude, mean GVI predictions on 3D-space to see if the data distribution is spherical.

As silhouette score remains similar with different number of clusters as shown in Figure 4.4 and Figure 4.5, elbow method is used to determine the number of clusters for Kmeans clustering. The inertia of clusters are plotted against the number of clusters in Figure 4.7 where the inflection point ('elbow') is chosen to be the number of clusters. In this case, the number of clusters is chosen to be 4.

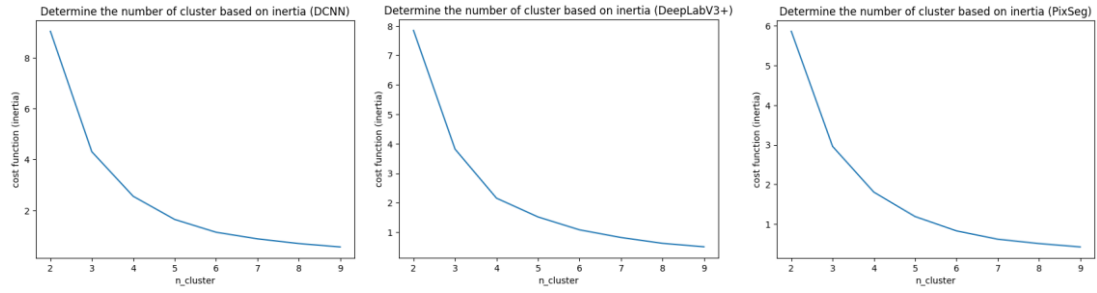


Figure 4.7 Determine the number of clusters with elbow method.

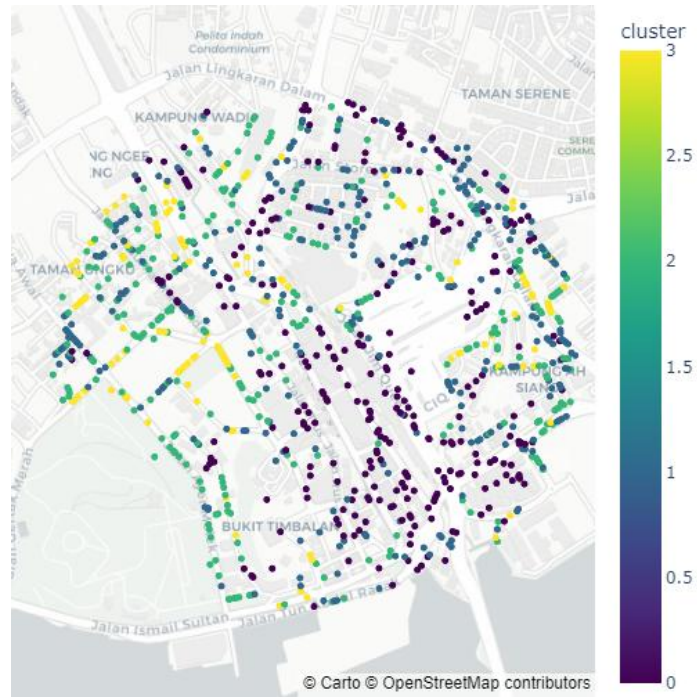


Figure 4.8 Visualization of hierarchical clusters (DCNN, cluster=4).

Figure 4.8 shows an example of clustering results based on DCNN GVI predictions and location of sampling points visualised on map. As DCNN has the best performance in terms of accuracy, robustness and biasness, only its predictions are used for further clustering analysis in the following sections.

In the following section, the characteristics of each cluster are explored and analyzed in detail.



4.3.1 Cluster 0

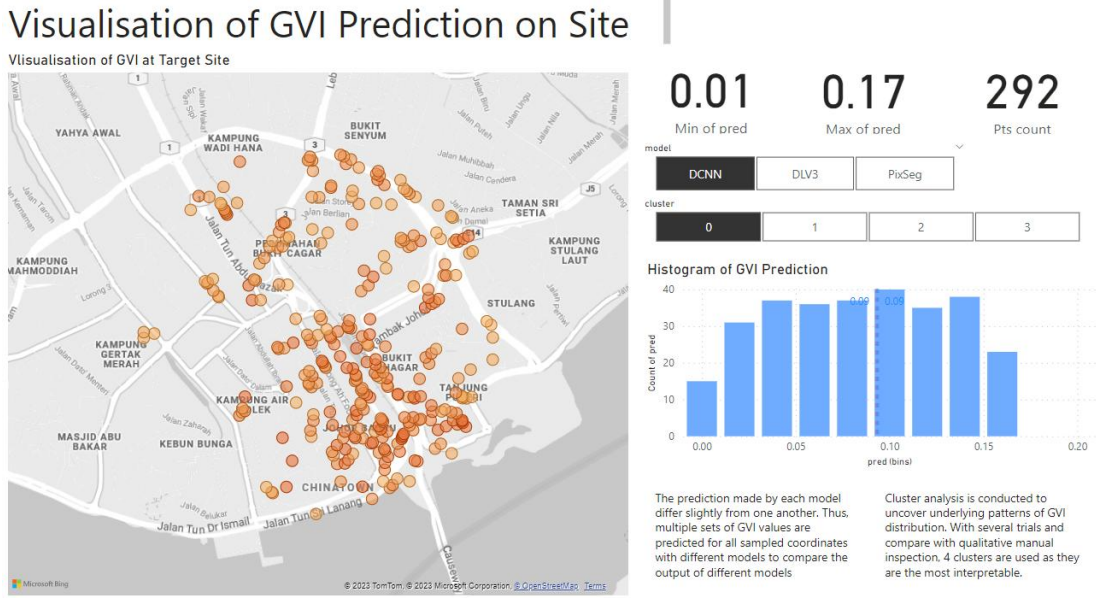


Figure 4.9 Visualization of cluster 0 for DCNN Kmeans clustering.

Cluster 0 has the lowest predicted GVI values. There are 292 spots where GVI is in the lowest range of 0.01 and 0.17. Their average and median GVI are as low as 0.09. From the map plot, we can observe that there are certain characteristics to where these low GVI spots are located.

For instance, they are often located on highways and main roads without any observable vegetation. Figure 4.10 highlights the vehicular roads where spots with low predicted GVI values from cluster 0 are located and Figure 4.11 illustrates sample GSV taken from these locations.



Figure 4.10 Roads that intersect with or adjacent to spots from cluster 0.



From Figure 4.10, we can notice that there are very few ..... While it is a lot harder to plant trees in these areas due to maintenance and arrangements issues, the presence of a lot of such spots can represent a problem in urban design as it creates too much very uncomfortable space for its users.



Figure 4.11 Sample GSV images taken from highways and main roads with very little observable vegetation.

While it is a lot harder to plant trees in these areas due to maintenance and arrangements issues, the presence of a lot of such spots can represent a problem in urban design as it creates too much very uncomfortable space for its users.

Other than highways and large vehicular roads, there are also certain zones, especially at the Southern part of the site with dense commercial zones as shown in Figure 4.12, with sample GSV images illustrated in Figure 4.13. Due to the high density of these areas and the lack of green space planning, these places have very low GVI in result.



Figure 4.12 Highlights on the city center with high density commercial area.



Figure 4.13 Sample GSV images taken from areas highlighted in Figure 4.12.

In conclusion, in Cluster 0, we can notice plenty urban spaces in the target site with very low predicted GVI values, with a lot of them on main road or highway and the densely populated commercial zone at the Southern part of the Johor Bahru city center. This illustrates possible fundamental flaws in the vehicle-centric and careless urban planning for the Johor Bahru city center without consideration for green spaces.

### 4.3.2 Cluster 1

#### Visualisation of GVI Prediction on Site

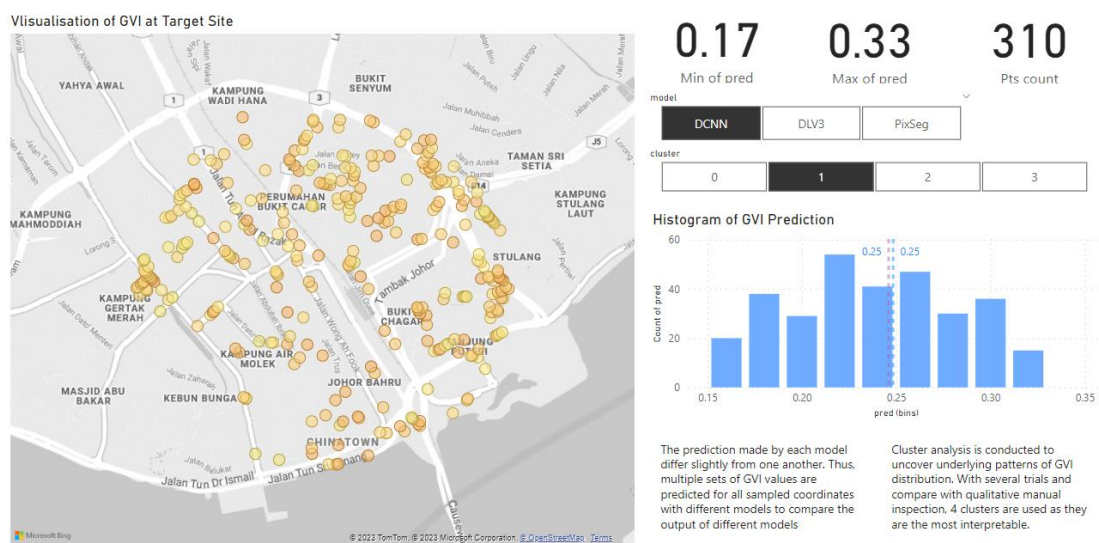


Figure 4.14 Visualization of cluster 1 for DCNN Kmeans clustering.

Cluster 1 has higher predicted GVI values than Cluster 0. There are 310 spots where GVI is in the lower range of 0.17 and 0.33. Their average and median GVI are both 0.25. From the map plot, we can observe Cluster 1 is much more evenly scattered compared with Cluster 0. This shows that the GVI values in Cluster 1 is more commonly experienced in the Johor Bahru City Center.

In fact, by inspecting the GSV images in Cluster 1, we can observe that the spots in Cluster 1 are mostly in active commercial and residential areas that makes up a very big part of our experience in a place. In Figure 4.16 and Figure 4.17, GSV from commercial areas and residential marked in Figure 4.15 are illustrated respectively.

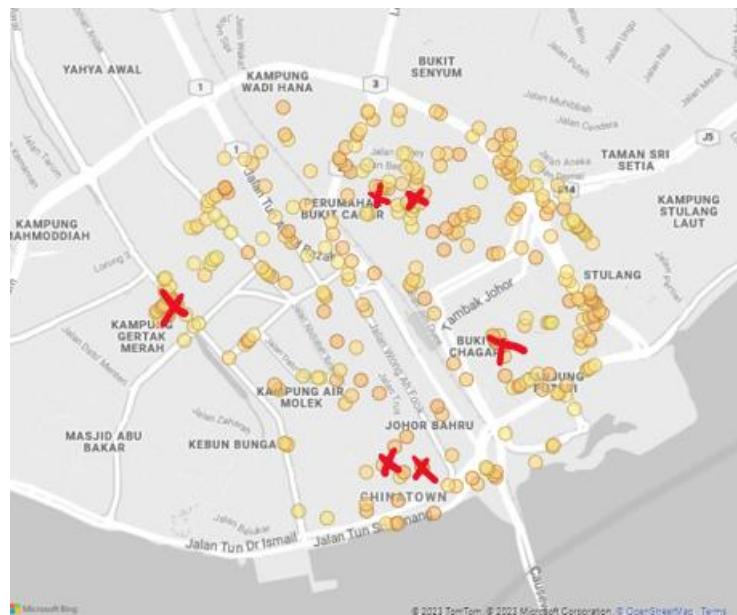


Figure 4.15 Indication of the sampling location for GSV images displayed in Figure 4.16 and Figure 4.17.





Figure 4.16 Sample GSV images from commercial areas marked in Figure 4.15.



Figure 4.17 Sample GSV images from residential areas marked in Figure 4.15.

In conclusion, we can notice sampling spots from Cluster 1 scattering evenly across the Johor Bahru city center, especially active commercial and residential areas, forming a major part of the experience of the urban space users. In these places with GVI in the range of 0.17 and 0.33, there are plenty of green views compared with the spots in Cluster 0 with green belts, street trees, etc.

### 4.3.3 Cluster 2

#### Visualisation of GVI Prediction on Site

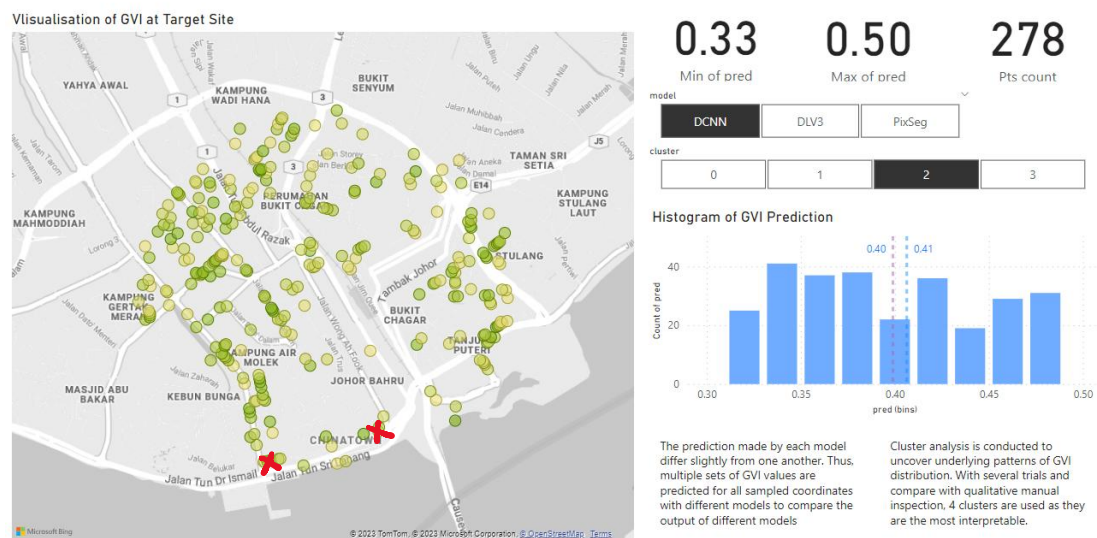


Figure 4.18 Visualization of Cluster 2 for DCNN Kmeans clustering.

Cluster 2 has the second highest predicted GVI values. There are 278 spots where GVI is in the higher range of 0.33 and 0.50. Their average and median GVI are 0.41 and 0.40 respectively. From the map plot, we can observe Cluster 2 is much more focused at the North, East and West part of the site.

By visualizing the aerial view of the plot, we can realize that this is the case as the distribution of Cluster 3 points are usually located adjacent to the green pocket spaces or belts in the city center. Due to the high density of man-made structures and buildings at the Southern side, it is harder to incorporate these spaces at the Southern side. Figure 4.19 displays the aerial view and grayscale map where Cluster 3 points are plotted on to illustrate the observation mentioned above.



Figure 4.19 displays the aerial view and grayscale map where Cluster 3 points are plotted on.

Compared with large scale parks or forests, these small green areas are more effective in permeating the city and can introduce green views to the daily to more places. Figure 4.21 illustrates GSV of places where these green pocket spaces increase the predicted GVI of the spot. Indication of where images in Figure 4.21 are sampled from is displayed in map-plot in Figure 4.20.



Figure 4.20 Indication of the sampling location for GSV images displayed in Figure 4.21.



Figure 4.21 Sample GSV images marked in Figure 4.20.

Last but not least, there is an interesting observation in the Chinatown street located at the densest commercial area, i.e. despite the small street, they managed to incorporate small street trees, thereby significantly increase the predicted GVI values on the street. This shows that the dense commercial areas in Cluster 0 have the potential to increase their GVI with more street trees despite the lack of space. In Figure 4.22, GSV image of the street incorporating street trees in the walkway on the Chinatown street.





Figure 4.22 GSV image of the street incorporating street trees in the walkway on the Chinatown street. Its location is marked on the map on the left.

#### 4.3.4 Cluster 3

##### Visualisation of GVI Prediction on Site

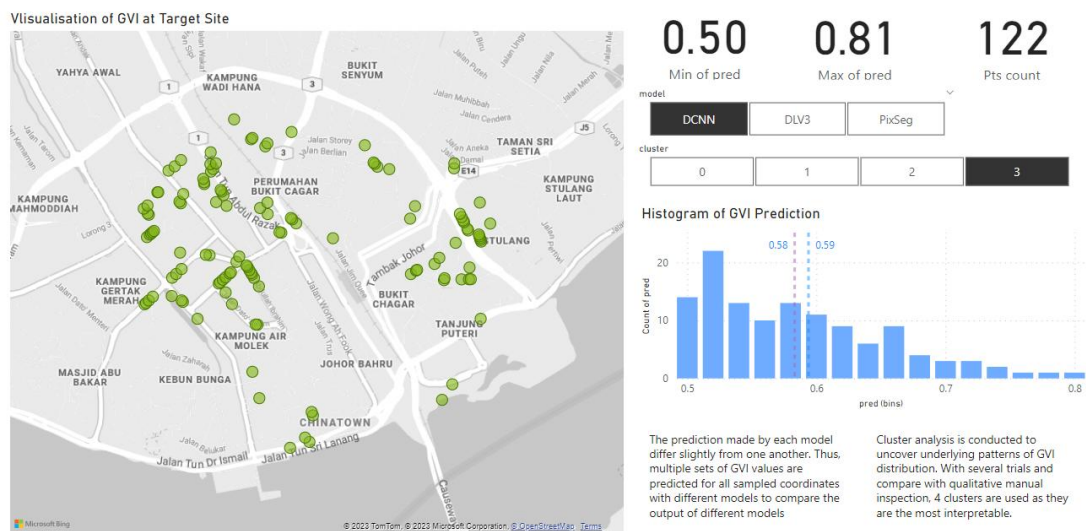


Figure 4.23 Visualization of Cluster 3 for DCNN Kmeans clustering.

Cluster 3 has the highest predicted GVI values. There are 122 spots where GVI is in the higher range of 0.50 and 0.81. Their average and median GVI are 0.59 and 0.58 respectively. From the map plot, we can notice Cluster 3 to have a very similar distribution pattern compared with Cluster 2 as shown in Figure 4.24.

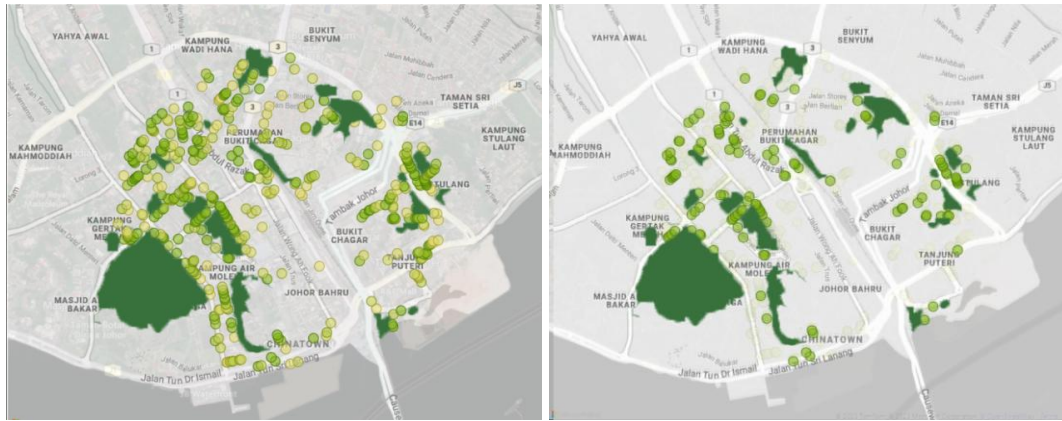


Figure 4.24 Comparison of Cluster 3 (right) distribution compared with Cluster 2 (left).

Nonetheless, by manually inspecting the GSV images for Cluster 3, we can see that there is a differentiator between data points in Cluster 3 and Cluster 2. In Cluster 3, data points are mostly located at areas that have lower density, smaller roads and are less developed. Figure 4.26 illustrates GSV samples of Cluster 3. An indication of where images in Figure 4.26 are sampled from is displayed in map-plot in Figure 4.25.



Figure 4.25 Indication of the sampling location for GSV images displayed in Figure 4.26.





Figure 4.26 Sample GSV images marked in Figure 4.25.

### 4.3.5 Clustering Analysis Conclusion

In conclusion, the clustering analysis of the GVI values in Johor Bahru city center provides several key insights regarding the distribution of green views and urban design considerations:

Cluster 0 represents urban spaces with very low predicted GVI values. These spots are mainly located on highways and main roads without observable vegetation. The presence of numerous low GVI spots in these areas highlights a fundamental flaw in vehicle-centric and careless urban planning that neglects the need of green spaces. It creates uncomfortable spaces for users and poses challenges for planting trees due to maintenance and arrangement issues.

Cluster 1 consists of spots with higher predicted GVI values compared to Cluster 0. These spots are more evenly scattered throughout the city center, particularly in active commercial and residential areas. These areas contribute significantly to the overall experience of urban space users. Cluster 1 spots exhibit a higher presence of green views, including green belts, street trees, and other forms of vegetation.

Cluster 2 includes spots with the second-highest predicted GVI values. They are primarily concentrated in the North, East, and West parts of the city center.

Cluster 2 spots tend to be adjacent to green pocket spaces or belts, effectively permeating the city with greenery. These smaller green areas play a crucial role in enhancing the predicted GVI of the surrounding spots, offering green views in various locations. Incorporating more street trees in dense commercial areas, like the Chinatown street, has the potential to increase GVI despite limited space.

Cluster 3 represents spots with the highest predicted GVI values. Similar to Cluster 2, these spots are distributed in a comparable pattern, primarily in less dense and less developed areas with smaller roads. Although they share a distribution pattern with Cluster 2, the differentiating factor is the lower density and less developed nature of Cluster 3 areas. These spots offer a higher abundance of green views and contribute to a higher GVI.

Table 4.2 shows the mean GVI predictions and number of samples of each cluster for DCNN's GVI predictions. From the table, we can see that Cluster 0 and Cluster 1 is more predominant in the target site compared with that of Cluster 2 and 3. This shows that there are still many room of improvements to incorporate Green View in Johor Bahru city center.

Table 4.2 DCNN KMeans clusters with their respective mean GVI predictions.

Cluster	Number of Samples	Mean GVI Predictions
0	292	0.012675
1	310	0.171307
2	278	0.327357
3	122	0.501539

While some of the reasons behind the dominance of Cluster 0 and Cluster 1 are due to deep rooted urban planning issue that cannot be easily reversed such as too many highways and main roads, lack of green space incorporation in older streets, there are ways that we can do to optimize GVI values in target site based on the existing conditions. For instance, from Cluster 2, we realize that the inclusion of

green belts, street trees and small green pocket areas, urban designers can significantly enhance the GVI values and overall urban experience for residents and visitors. This illustrates how important it is to develop effective methods for us to analyze green views in target site and develop appropriate solutions to improve GVI accordingly.

### 4.3 Dashboard

As part of this project, a comprehensive analysis was conducted to assess the distribution of green views within the Johor Bahru city center. The dashboard provides a user-friendly interface that allows stakeholders and urban planners to explore the distribution of Green View Index (GVI) values across the target site while inspecting the errors and bias underlying the prediction models. In the following figures, developed dashboards are presented and elaborated.

#### Model Error Analysis

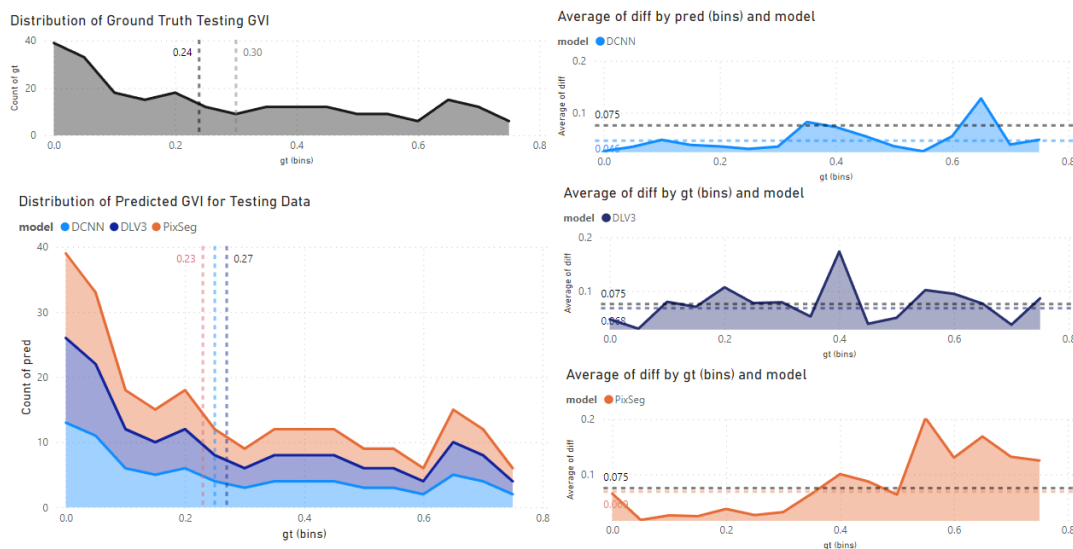


Figure 4.27 This dashboard investigates the error of each model at different predicted GVI values.

In the first chart on the top left corner, the distribution of ground truth GVI values for test data is plotted to be compared with GVI predictions of each model in

the stacked chart below it. The 2 constant dotted lines in the ground truth GVI distribution chart represent median and mean respectively while the dotted lines in GVI prediction distribution chart represent the mean for each model prediction. With this, we can get a general idea of how the distribution of GVI predictions of each model compares with the ground truth.

On the other hand, the errors of each prediction model are studied with the charts on the right-hand side. The absolute error between GVI prediction and GVI ground truth is plotted against the GVI ground truth to investigate the errors for each model at different GVI levels. These charts allow us to break down and analyze the accuracy of models at different situations, making the models more interpretable.

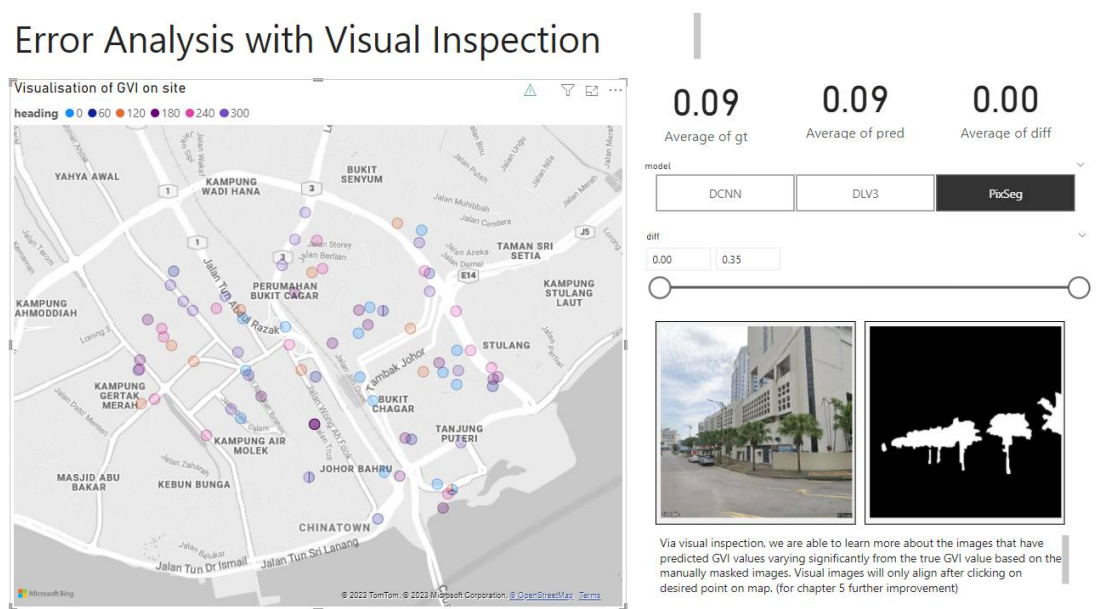


Figure 4.28 This dashboard visualizes the GSV image and label to allow more detailed error analysis of model with visual inspection.

Visual inspection of test data is another essential key for model development. By looking into the original GSV image and label data and comparing them with the predicted GVI, one can get a better idea about the possible reasons leading to error in prediction.

The map plot on the left visualizes the points and headings of GSV test data. By selecting or clicking on the point that we wish to inspect, we are able to view its

respective GSV image and label and gauge the underlying problems leading to prediction error. The respective ground truth GVI, prediction and their difference are displayed on the cards.

To enable more flexibility in error inspection, two slicers are added to control the scope of data. For instance, if one wants to review the error larger than 0.20 in DCNN model predictions, one can adjust the slicer settings accordingly. This makes the work of inspection much more convenient as one is able to focus the scope of review to according to their needs.

## Visualisation of GVI Prediction on Site

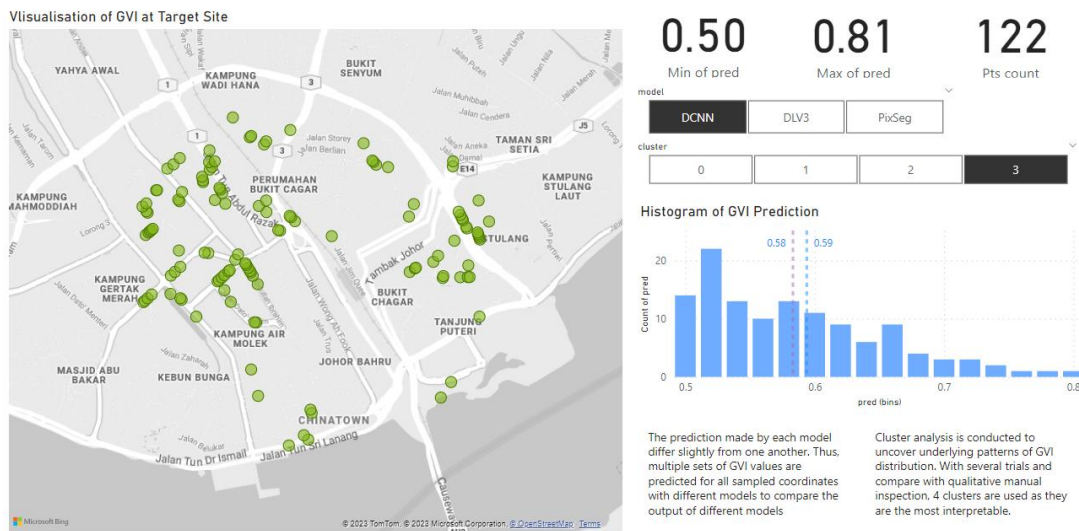


Figure 4.29 This dashboard visualizes the GVI predictions of all GSV data collected on site.

Through this dashboard, users can visualize the spatial distribution of the clusters on an interactive map. The map highlights the locations of spots within each cluster and provides insights into their respective GVI values. The greener a point is, the higher its GVI prediction; the redder a point, the lower its GVI prediction. On the right corner of the dashboard, the minimum and maximum GVI prediction, along with the number of point locations are visualized to provide a basic idea of the GVI predictions of the visualized data points. From the histogram, we can also observe the distribution of predicted GVI values for the visualized data.

The slicers are established based on “models” and “cluster”, with the former enabling us to visualize the predictions based on different models and the latter being used to carry out clustering analysis.

#### **4.4 Chapter Summary**

In conclusion, among DCNN, DeepLabV3+ and Pixel Segmentation models trained to predict GVI, DCNN has the greatest performance in terms of accuracy and robustness with. In terms of inference time, DCNN has a moderate inference time of 43.87s for 1000 predictions, which is in between 9.99s and 121.83s for Pixel Segmentation model and DeepLabV3+ respectively. Therefore, DCNN is deemed to have the best overall performance.

For clustering analysis, with experimentation on various clustering approaches, we find out that Kmeans with 4 clusters is the most suitable clustering approach for the GVI prediction in Johor Bahru city center. By applying this clustering approach on the DCNN GVI predictions, we can notice patterns in GVI distribution in target site. For instance, Cluster 0 with low GVI predictions are mainly focused on highways and the South part of the site with highly dense commercial buildings; Cluster 1 with moderately low GVI are the most evenly scattered cluster across the site; Cluster 2 with second highest GVI predictions are usually adjacent to green pocket spaces and belts; Cluster 3 with the highest GVI predictions are located in the less developed areas within the city center.

By carrying out clustering analysis, one can understand the underlying patterns that affect how much the people in the city makes experience greens in their daily lives and thereby generate appropriate solutions accordingly to optimize GVI and improve urban spatial experience in the target site.

## **CHAPTER 5**

### **CONCLUSION**

#### **5.1 Contribution**

In evaluating multiple models for Green View Index (GVI) prediction, i.e. pixel segmentation, DCNN model, and DeepLabV3+ model, this study provides valuable insights into the accuracy, inference time, and potential biases associated with each approach. With information on the performance of these methods, urban planners can select the most appropriate model for GVI prediction based on specific requirements and constraints.

The predicted GVI in selected site, Johor Bahru city center is clustered and analysed to reveal distinct patterns and trends within the GVI data. These clusters represent categories based on predicted GVI ranges, generating invaluable insights of green views across the city center, thereby contributing to inform appropriate solutions to optimize it. The interactive dashboard developed as part of this project allows stakeholders and urban planners to visualize and explore these clusters, gaining a deeper understanding of the spatial distribution of green spaces.

In short, this project offers a comprehensive understanding of the current state of green views in the Johor Bahru city center. The findings provide valuable guidance for urban planners in optimizing green space allocation, identifying areas in need of improvement, and promoting sustainable and user-friendly urban environments. The experience and insights generated from this project can be generalized to understand the state of urban green coverage in other cities in Malaysia.

## 5.2 Limitations of Project

In this project, we have visualized the GVI values in Johor Bahru city center that enables future research. Nonetheless, it also comes with several limitations.

Firstly, the scope of the project is too small. As the current project only covers a radius of 1000m, it only includes a very small part in Johor Bahru. The small scope does not allow us to uncover more patterns that can further inform urban planning. Besides, due to the limitations of Google API, the range of the study site is set to be a circle with constant radius. This arbitrary site boundary does not allow for more nuanced analysis on factors that can result in differences of GVI, e.g., local governance, zoning, socioeconomic level of the site, etc. A larger study site in GIS can be used to conduct more comprehensive study on a larger scale. Complementary information such as zoning and socioeconomic levels can be juxtaposed to the GVI of site to extract insights for urban planning.

Regarding the sampling process, there is an important limitation too. As the GSV images are retrieved by random coordinates within the set site boundary, the sampling does not consider the distance between sampling points. This method is suboptimal as it can either (1) not cover the study site adequately for comprehensive analysis or (2) taking too many samples at similar points which results in bias. This can be optimized by integrating GIS information consisting of street information and setting constraints such as distances between sampling points on the same street to be within a particular range.

For the calculation of GVI, the limitation lies in the variation of target data as they are created by manually tracing vegetation in Photoshop. This can introduce a lot of noise and bias for the model developed for GVI computation, which is especially so when we try to scale up and include more data. This can be improved by establishing a rigorous selection method to follow when manually selecting vegetation. As GVI is point data, they can be aggregated to produce a weighted mean GVI of an area to make them more interpretable for the stakeholders.



As for explorative analysis on each cluster, they are mostly qualitative instead of quantitative due to the complexity of retrieving relevant layers of data such as zoning of site, road width and length in digital format. Due to the lack of extra layers of data, it is difficult to carry out quantitative study on how GVI distribution relates to other features. This has significantly limited the comprehensiveness of the quantitative elements in this study.

In conclusion, there are multiple limitations in terms of the scope of study, sampling methods, model development for GVI calculation and clustering analysis that can be improved in further studies.

### **5.3 Future Improvements**

Based on the limitations established, several improvements can be made in the further development of the project. Firstly, a larger site can be used to uncover more patterns and contexts behind distribution of GVI. Second, a GIS model including street information can be used to optimize the sampling method by setting the minimum and maximum distance between sampling locations, thereby reducing bias introduced. Thirdly, a more rigorous and formal process for ground truth generation when masking greeneries manually will be established to reduce the man-made variation. Finally, more features should be included in the study to increase the comprehensiveness of the study of GVI, e.g. road width, estate price, zoning, etc.

## REFERENCES

- Abdul Aziz, N.A., Konijnendijk, C., Maruthaveeran, S., Nilsson, K., 2011. Greenspace Planning and Management in Klang Valley, Peninsular Malaysia. *Journal of Arboriculture* 37, 99–107. <https://doi.org/10.48044/jauf.2011.014>
- Aziz, N. A. A. (2012). Green space use and management in Malaysia. *Forest & Landscape*.
- Badrinarayanan, V., Kendall, A., Cipolla, R., 2017. SegNet: A Deep Convolutional Encoder-Decoder Architecture for Image Segmentation. *IEEE Transactions on Pattern Analysis and Machine Intelligence* 39, 2481–2495. <https://doi.org/10.1109/TPAMI.2016.2644615>
- Cai, B.Y., Li, X., Seiferling, I., Ratti, C., 2018. Treepedia 2.0: Applying Deep Learning for Large-Scale Quantification of Urban Tree Cover, in: 2018 IEEE International Congress on Big Data (BigData Congress). Presented at the 2018 IEEE International Congress on Big Data (BigData Congress), IEEE, San Francisco, CA, pp. 49–56. <https://doi.org/10.1109/BigDataCongress.2018.00014>
- Chen, L.-C., Zhu, Y., Papandreou, G., Schroff, F., Adam, H., 2018. Encoder-Decoder with Atrous Separable Convolution for Semantic Image Segmentation, in: Ferrari, V., Hebert, M., Sminchisescu, C., Weiss, Y. (Eds.), *Computer Vision – ECCV 2018, Lecture Notes in Computer Science*. Springer International Publishing, Cham, pp. 833–851. [https://doi.org/10.1007/978-3-030-01234-2\\_49](https://doi.org/10.1007/978-3-030-01234-2_49)
- Cheng, L., Chu, S., Zong, W., Li, S., Wu, J., Li, M., 2017. Use of Tencent Street View Imagery for Visual Perception of Streets. *ISPRS International Journal of Geo-Information* 6, 265. <https://doi.org/10.3390/ijgi6090265>

- Dong, R., Zhang, Y., Zhao, J., 2018. How Green Are the Streets Within the Sixth Ring Road of Beijing? An Analysis Based on Tencent Street View Pictures and the Green View Index. *International Journal of Environmental Research and Public Health* 15, 1367. <https://doi.org/10.3390/ijerph15071367>
- He, K., Zhang, X., Ren, S., Sun, J., 2015. Deep Residual Learning for Image Recognition.
- Hu, J., Zhang, L., Liang, W. and Wang, Z. (2009) ‘Incipient mechanical fault detection based on multifractal and MTS methods’, *Petroleum Science*, 6(2), pp. 208–216. Zhang, J., Hu, A., 2022. Analyzing green view index and green view index best path using Google street view and deep learning. *Journal of Computational Design and Engineering* 9, 2010–2023. <https://doi.org/10.1093/jcde/qwac102>
- James, P., Tzoulas, K., Adams, M.D., Barber, A., Box, J., Breuste, J., Elmqvist, T., Frith, M., Gordon, C., Greening, K.L., Handley, J., Haworth, S., Kazmierczak, A.E., Johnston, M., Korpela, K., Moretti, M., Niemelä, J., Pauleit, S., Roe, M.H., Sadler, J.P., Ward Thompson, C., 2009. Towards an integrated understanding of green space in the European built environment. *Urban Forestry & Urban Greening* 8, 65–75. <https://doi.org/10.1016/j.ufug.2009.02.001>
- Kanniah, K.D., 2017. Quantifying green cover change for sustainable urban planning: A case of Kuala Lumpur, Malaysia. *Urban Forestry & Urban Greening* 27, 287–304. <https://doi.org/10.1016/j.ufug.2017.08.016>
- Kasim, J. A., Yusof, M. J. M., & Shafri, H. Z. M. (2019). Monitoring urban green space (UGS) changes by using high resolution aerial imagery: A case study of Kuala Lumpur, Malaysia. *Pertanika J. Sci. Technol*, 27, 1971-1990.
- Katole, A.L., Yellapragada, K.P., Bedi, A.K., Kalra, S.S., Siva Chaitanya, M., 2015. Hierarchical Deep Learning Architecture for 10K Objects Classification, in: *Computer Science & Information Technology ( CS & IT )*. Presented at the

- Second International Conference on Computer Science & Engineering, Academy & Industry Research Collaboration Center (AIRCC), pp. 77–93. <https://doi.org/10.5121/csit.2015.51408>
- Kumakoshi, Y., Chan, S., Koizumi, H., Li, X., Yoshimura, Y., 2020. Standardized Green View Index and Quantification of Different Metrics of Urban Green Vegetation. *Sustainability* 12, 7434. <https://doi.org/10.3390/su12187434>
- LeCun, Y., & Bengio, Y. (1995). Convolutional networks for images, speech, and time series. *The handbook of brain theory and neural networks*, 3361(10), 1995.
- Lee, A.C.K., Maheswaran, R., 2011. The health benefits of urban green spaces: a review of the evidence. *Journal of Public Health* 33, 212–222. <https://doi.org/10.1093/pubmed/fdq068>
- Li, X., Zhang, C., Li, W., Ricard, R., Meng, Q., Zhang, W., 2015. Assessing street-level urban greenery using Google Street View and a modified green view index. *Urban Forestry & Urban Greening* 14, 675–685. <https://doi.org/10.1016/j.ufug.2015.06.006>
- Long, J., Shelhamer, E., & Darrell, T. (2015). Fully convolutional networks for semantic segmentation. In *Proceedings of the IEEE conference on computer vision and pattern recognition* (pp. 3431-3440).
- Long, Y., Liu, L., 2017. How green are the streets? An analysis for central areas of Chinese cities using Tencent Street View. *PLOS ONE* 12, e0171110. <https://doi.org/10.1371/journal.pone.0171110>
- Luo, J., Zhai, S., Song, G., He, X., Song, H., Chen, J., Liu, H., Feng, Y., 2022. Assessing Inequity in Green Space Exposure toward a “15-Minute City” in Zhengzhou, China: Using Deep Learning and Urban Big Data. *International Journal of Environmental Research and Public Health* 19, 5798. <https://doi.org/10.3390/ijerph19105798>

- Masum, K.M., Mansor, A., Sah, S.A.M., Lim, H.S., 2017. Effect of differential forest management on land-use change (LUC) in a tropical hill forest of Malaysia. *Journal of Environmental Management* 200, 468–474. <https://doi.org/10.1016/j.jenvman.2017.06.009>
- Minaee, S., Boykov, Y., Porikli, F., Plaza, A., Kehtarnavaz, N., Terzopoulos, D., 2022. Image Segmentation Using Deep Learning: A Survey. *IEEE Transactions on Pattern Analysis and Machine Intelligence* 44, 3523–3542. <https://doi.org/10.1109/TPAMI.2021.3059968>
- Nor, A.N.M., Abdullah, S.A., 2019. Developing Urban Green Space Classification System Using Multi-Criteria: The Case of Kuala Lumpur City, Malaysia. *Journal of Landscape Ecology* 12, 16–36. <https://doi.org/10.2478/jlecol-2019-0002>
- Padilla, R., Netto, S. L., & Da Silva, E. A. (2020, July). A survey on performance metrics for object-detection algorithms. In 2020 international conference on systems, signals and image processing (IWSSIP) (pp. 237-242). IEEE.
- Pauleit, S., 2003. Urban street tree plantings: identifying the key requirements. *Proceedings of the Institution of Civil Engineers - Municipal Engineer* 156, 43–50. <https://doi.org/10.1680/muen.2003.156.1.43>
- Rusli, N., Ludin, A.N.M., n.d. (PDF) Evaluation of Open Space and Recreation Area in Johor Bahru Tengah Municipal Council [WWW Document]. URL [https://www.researchgate.net/publication/327200128\\_Evaluation\\_of\\_Open\\_Space\\_and\\_Recreation\\_Area\\_in\\_Johor\\_Bahru\\_Tengah\\_Municipal\\_Council](https://www.researchgate.net/publication/327200128_Evaluation_of_Open_Space_and_Recreation_Area_in_Johor_Bahru_Tengah_Municipal_Council) (accessed 12.20.22).
- Schwaab, J., Meier, R., Mussetti, G., Seneviratne, S., Bürgi, C., Davin, E.L., 2021. The role of urban trees in reducing land surface temperatures in European cities. *Nat Commun* 12, 6763. <https://doi.org/10.1038/s41467-021-26768-w>

- Seiferling, I., Naik, N., Ratti, C., Proulx, R., 2017. Green streets – Quantifying and mapping urban trees with street-level imagery and computer vision. *Landscape and Urban Planning* 165, 93–101. <https://doi.org/10.1016/j.landurbplan.2017.05.010>
- Sundara Rajoo, K., Karam, D.S., Abdu, A., Rosli, Z., James Gerusu, G., 2021. Urban Forest Research in Malaysia: A Systematic Review. *Forests* 12, 903. <https://doi.org/10.3390/f12070903>
- Wang, J., Sun, K., Cheng, T., Jiang, B., Deng, C., Zhao, Y., Liu, D., Mu, Y., Tan, M., Wang, X., Liu, W., Xiao, B., 2021. Deep High-Resolution Representation Learning for Visual Recognition. *IEEE Trans. Pattern Anal. Mach. Intell.* 43, 3349–3364. <https://doi.org/10.1109/TPAMI.2020.2983686>
- Xia, Y., Yabuki, N., Fukuda, T., 2021. Development of a system for assessing the quality of urban street-level greenery using street view images and deep learning. *Urban Forestry & Urban Greening* 59, 126995. <https://doi.org/10.1016/j.ufug.2021.126995>
- Yu, H., Zhou, Y., Wang, R., Qian, Z., Knibbs, L.D., Jalaludin, B., Schootman, M., McMillin, S.E., Howard, S.W., Lin, L.-Z., Zhou, P., Hu, L.-W., Liu, R.-Q., Yang, B.-Y., Chen, G., Zeng, X.-W., Feng, W., Xiang, M., Dong, G.-H., 2021. Associations between trees and grass presence with childhood asthma prevalence using deep learning image segmentation and a novel green view index. *Environmental Pollution* 286, 117582. <https://doi.org/10.1016/j.envpol.2021.117582>
- Yuan, Y., Chen, X., & Wang, J. (2020, August). Object-contextual representations for semantic segmentation. In *European conference on computer vision* (pp. 173-190). Springer, Cham.
- Zhang, Y., Dong, R., 2018. Impacts of Street-Visible Greenery on Housing Prices: Evidence from a Hedonic Price Model and a Massive Street View Image

Dataset in Beijing. ISPRS International Journal of Geo-Information 7, 104.  
<https://doi.org/10.3390/ijgi7030104>

Zhang, J., Hu, A., 2022. Analyzing green view index and green view index best path using Google street view and deep learning. Journal of Computational Design and Engineering 9, 2010–2023. <https://doi.org/10.1093/jcde/qwac102>

Zhao, H., Shi, J., Qi, X., Wang, X., Jia, J., 2017. Pyramid Scene Parsing Network, in: 2017 IEEE Conference on Computer Vision and Pattern Recognition (CVPR). Presented at the 2017 IEEE Conference on Computer Vision and Pattern Recognition (CVPR), IEEE, Honolulu, HI, pp. 6230–6239. <https://doi.org/10.1109/CVPR.2017.660>

## ARCHIVE

For the code details, refer to the repository link: [xian-jun/Green-View-Index---Johor-Bahru:](https://github.com/xian-jun/Green-View-Index---Johor-Bahru)  
[A study of how green view index in Johor Bahru with Google Street View Image.](https://github.com/xian-jun/Green-View-Index---Johor-Bahru)  
[\(github.com\)](https://github.com/xian-jun/Green-View-Index---Johor-Bahru)